POSITIONING PERFORMANCE OF SINGLE-FREQUENCY GNSS RECEIVERS USING AUSTRALIAN REGIONAL IONOSPHERIC CORRECTIONS

Wenjiao Liu

Principal supervisor: Prof. Yanming Feng

Associate supervisor: Dr. Hasmukh Morarji

Submitted in fulfilment of the requirements for the degree of
Master of Information Technology (Research)

Data Science Discipline
Science and Engineering Faculty
Queensland University of Technology
2016

Keywords

Regional ionospheric map, station-based ionospheric correction, single-frequency PPP, SPP, decimetre positioning, coordinate space representation

Abstract

Single-frequency (SF) global positioning system (GPS) receivers have the potential to become an accurate alternative to high-end dual frequency receivers for many applications, such as geographical information system (GIS) data collections, vehicle positioning for lane-level safety and traffic management applications. For a SF receiver to achieve positioning precision of decimetre level, ionosphere delay is the main bottleneck among all error sources. The IGS-released global ionospheric map (GIM) provides for ionosphere corrections. However, the GIM corrections neither are available for real-time applications, nor have the accuracy required to enable single frequency decimetre positioning.

With around 200 reference stations, Australian regional ionospheric corrections are generated with high temporal and spatial resolution of both slant and vertical total electron contents. This thesis describes the unified station-based precise point positioning (PPP) ionosphere estimation method, which preserves the integer nature for carrier phase ambiguity resolutions. In order to achieve decimetre or higher precision, error sources including differential code biases (DCB), solid earth tide, phase centre offset and windup are taken into consideration, in addition to the adoption of precise orbits and clocks. With respect to applying the corrections, the coordinate space representation (CSR) method is proposed in this work, as a simple and pragmatic solution for mobile phone users without GNSS raw data in the data processing.

With the ionospheric corrections generated for 1 January 2014, the evaluation is performed with both single point positioning (SPP) and single frequency precise point positioning (SF-PPP) modes, based on the modifications to the RTKLIB software platform. The SPP solutions from 25 selected reference receivers have shown the decimetre root mean square (RMS) accuracy to be better than 19 cm for the east/north directions and 55 cm for the up component. With the same data sets and receivers, the SF-PPP mode yields the RMS accuracy of better than 10 cm and 25 cm for the horizontal and vertical components respectively. As a result, distinct improvement on positioning performance is demonstrated with Australian ionospheric corrections, and decimetre precision is demonstrated. The described road

scenario experiments demonstrate the significance of our Australian slant ionospheric correction products to mass-market applications. The experiments indicate that even low-cost receiver users such as car drivers are able to achieve sub-metre, or even decimetre positioning precision, as long as the slant ionospheric correction is accessed. Finally, CSR method is demonstrated to be pragmatic and have potential to address the traps that will be met in real applications.

Table of Contents

List of Figures

List of Tables

List of Abbreviations

A-GPS: assisted-GPS
AR: ambiguity resolution
BDS: Chinese BeiDou satellite
CODE: orbit determination in Europe
CORS: continuously operating reference station
CSR: coordinate space representation
DCB: differential code biases
DD: double difference
DF: dual-frequency
DGNSS: differential GNSS
EGNOS: European geostationary navigation overlay system
ENU: east, north, up
GAGAN: Indian GPS aided GEO augmented navigation
GAL: European Galileo navigation system
GEO: geostationary earth orbit
GIM: global ionosphere map
GIS: geographical information system
GLO: Russian GLONASS system
GNSS: global navigation satellite system
GPS: global positioning system
GSA: European GNSS agency
IGS: international GNSS service
IONEX: ionosphere map exchange format
IPP: ionosphere pierce point
IRNSS: Indian regional navigation satellite system
ITS: intelligent transport systems
JPL: jet propulsion laboratory
KIM: Klobuchar ionospheric model
LBS: location-based service
LOS: line of sight
MSAS: Japanese multi-functional satellite augmentation system
OSR: observation space representation
PNT: positioning, navigation, timing
PPP: precise point positioning
QZSS: Japan's quasi zenith satellite system
RIM: regional ionospheric map
RMS: root mean square
RNSS: regional navigation satellite system
RTCM: radio technical commission for maritime services
RTK: real-time kinematic
SBAS: satellite-based augmentation system
SD: single difference
SF: single-frequency
SF-PPP: single-frequency precise point positioning
SHF: spherical harmonic function
SIM: station-based ionospheric map
SPP: single point positioning
SPS: standard positioning service

SSR: state space representation

STD: standard deviation

TEC: total electron content

TECU: TEC unit

UAV: unmanned aerial vehicle

WAAS: wide area augmentation system

ZTD: zenith tropospheric delay

Statement of Original Authorship

The work contained in this thesis has not been previously submitted to meet requirements for an award at this or any other higher education institution. To the best of my knowledge and belief, the thesis contains no material previously published or written by another person except where due reference is made.

Signature:

Date: 1/12/2016

Acknowledgements

I would like to express my deep gratitude to my principal supervisor, Professor Yanming Feng, and also to my associate supervisor, Dr. Charles Wang for their kindness and great help during my Master's research. They have given me professional guidance in the research field, plus plenty of support, useful suggestions and sufficient resources since the first moment I started my research. Without these, I would not have made such great progress in my study. I have benefited a lot academically and personally for my study and future career.

Staff from Wuhan University have given me a lot of support in terms of software and experiment. I would also like to thank Dr. Shengfeng Gu and Fu Zheng.

I would also like to thank QUT for its great support, through its research facilities and the funding provided, both of which enabled me to successfully complete my Masters research and submit my thesis.

Finally, I would like to thank my family for their consistent encouragement and support, which has helped me overcome many difficulties and get through tough times.

Chapter 1: Introduction

This chapter gives the background of the problem to be explored (Section 1.1) and the major focuses and basic difficulties (Section 1.2) of the research. Section 1.3 defines the overarching objectives and specific aims. Section 1.4 describes the significance and the practical outcomes of this research and provides definitions of terms used. Section 1.5 outlines the remaining chapters of the thesis.

1.1 BACKGROUND

A global navigation satellite system (GNSS) refers to a constellation of satellites transmitting signals towards user receivers, providing positioning, navigation, and timing (PNT) services to global users. The global positioning system (GPS), the first and best-known GNSS, was proposed in 1973 for military use and has been fully operational since 1995, operated by the US Department of Defence. Nowadays, a number of GNSS systems are in operation or under development, including global constellations and regional-scale satellite systems. Global constellations include the Russian GLONASS (GLO), the European Union's Galileo (GAL), and the Chinese BeiDou satellite navigation system (BDS). In the regional scale, the satellite-based augmentation system (SBAS), the North American wide area augmentation system (WAAS), the European geostationary navigation overlay system (EGNOS), the Indian GPS aided GEO augmented navigation (GAGAN) and the Japanese multi-functional satellite augmentation system (MSAS) have emerged. In addition, there are two regional navigation satellite systems (RNSS): the Japan's quasi zenith satellite system (QZSS) and the Indian regional navigation satellite system (IRNSS). The current operational status, constellation details, frequencies and signals, and PNT services of various GNSS and RNSS systems are outlined in Table 1.1.

The GNSS technology, or satellite positioning technology, enables land, sea airborne and near-earth space users to determine their three-dimensional position, velocity and time (PVT), twenty-four hours a day in all weathers conditions, anywhere in the world. The existing GNSS applications are usually broadly grouped into three categories according to their requirements for the positioning performance

characteristics: mass-market, professional and safety-of-life. Mass-market users, such as personal mobile devices and road navigation devices, use low-end products that can offer the PNT accuracy to the level of metres to tens of metres. Professional users such as constructors, surveyors, mining and agriculture machineries, and scientists, usually use medium to high-end equipment. Their accuracy requirements can range from millimetres to decimetres, depending on applications. For instance, earth dynamic monitoring requires the accuracy of better than 1 cm; the land and marine surveying and machine automation requires the accuracy of centimetres. The safety-of-life market refers mainly to aviation navigation, which enables three-dimensional position determination for all phases of flight from departure, en route, and arrival, to airport surface navigation. The accuracy required can range from tens of metres down to decimetres, but high availability, integrity and continuity are important.

Table 1.1 Current operational GNSS and RNSS system

Coverage	System	Current / future frequencies and signals	Services	Current / future constellation
Global	GPS	L1: C/A, P, M L2: L2C, P, M L3, L5 L4: ionospheric correction	Standard Precise	32 satellites
	GLO	FDMA: L1, L2 CDMA: L3 (L1, L2) Interoperability CDMA: L1, L3, L5	Civilian Military	28 / 30 satellites
	GAL	E1, E5, E6, C-band	Open Commercial Regulated	14 / 30 satellites
	BDS	B1, B2, B3	Civilian Military	10 / 35 satellites
Regional	QZSS	L1, L1C, L1-SAIF, L2C, L5, LEX	Civilian	1 / 4 satellites
	IRNSS	L5, S-band	Standard Precise	7 satellites
	WAAS	L1, L5	Civilian	5 satellites
	EGNOS	L1, L5	Civilian	4 satellites
	GANAN	L1, L5	Civilian	3 satellites
	MSAS	L1, L5	Civilian	2 satellites

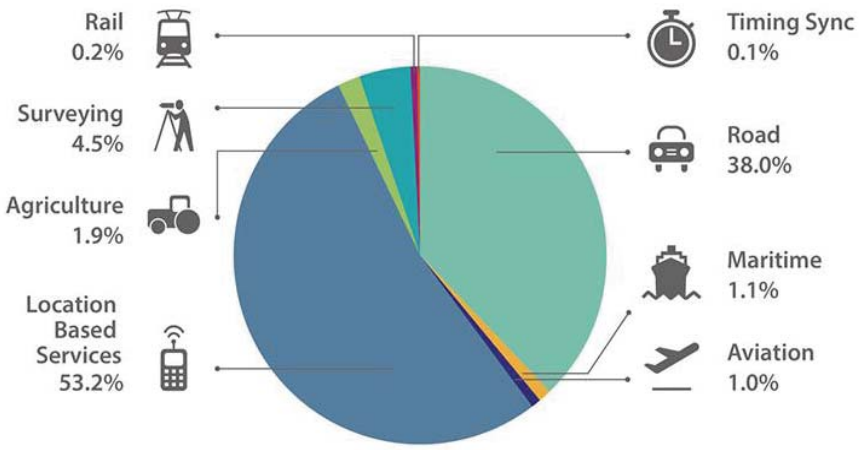

Figure 1.1 Cumulative distribution of global core revenue (value of GNSS chipsets) projected by the European GNSS Agency for the period 2013-2023 (GSA, 2015)

GNSS PNT applications can also be grouped in terms of industry sectors. The major sectors include transportation (further divided into road navigation, rail navigation, air navigation and marine navigation), location-based services (LBS), surveying and agriculture, as shown in Figure 1.1. According to the European GNSS agency (GSA), LBS and the road segment dominate cumulative GNSS revenues. In particular, the LBS market is driven by the booming sales of smartphones. Almost 3 billion mobile applications currently in use rely on positioning information, including map creating, advertising, safety and emergency, and social networking. The road market is led by the growth of in-vehicle devices. It primarily consists of navigation, logistics monitoring, traffic management, safety enhancing, and electronic tolling (GSA, 2015).

GPS standard positioning services (SPS) directly allow global positioning to the accuracy of 5-10 metres. This accuracy level meets the majority of LBS and road applications. Specific supporting services are required to meet requirements for higher accuracy or other performance parameters. SBAS systems are designed to meet mainly safety-of-life aviation requirements, which can improve GPS SPS accuracy to the level of a submetre to a few metres where a regional ground infrastructure is available. When the correction data from local continuously operating reference stations are available, the accuracy of 5 centimetres or better can be provided to the high-end users. This is offered by the single-based or network-based real-time kinematic (RTK) services. In recent years, some global companies, such as Trimble, Fugro and NavCom, have deployed precise point positioning (PPP) services regionally or globally. Both RTK and PPP services support high-end users.

The problem is that the PPP initialisation performance still depends on the density of the network, although it works anywhere in the globe. Another problem is that the high-end RTK or PPP services do not automatically cover all the users requiring the decimetre-level PNT services, simply because these users do not use high-end GNSS terminals and do not want to pay high on-going service charges.

Many emerging PNT applications across all the industry sectors or market categories require decimetre to submetre PNT accuracy. In the road sector, deployment of various vehicle to vehicle (V2V) and vehicle to infrastructure (V2I) safety applications requires the vehicle positioning accuracy of about 50 centimetres (Ansari et al., 2013; Green et al., 2013). This capability can estimate which lane a vehicle is travelling in and where it is in the lane. It provides support for individuals with intersection collision warning system to detect and warn drivers of approaching traffic at intersections. The lane change assistance functionality serves to alert bus and truck drivers of vehicles or obstacles in adjacent lanes, when the driver prepares to change lanes. Other applications requiring individual road safety include lane departure warning, rollover warning, and rear impact warning. In addition, lane-based traffic management requires knowledge of which lanes the vehicles are travelling in. Toll collection can also benefit from the lane-level precision. It is common that in one road segment, express lanes offer the privilege of higher speed than normal lanes offer. It is expected that tolling based on lanes and time periods travelled can be automated and independent of toll plazas, to save the construction cost of infrastructure for government and to increase the operational efficiency and convenience for individuals (http://www.itsoverview.its.dot.gov/). These road applications can be partially met by the SBASs in Europe and Northern America. Many vehicle safety applications developed in USA and Europe assume use of SBAS signals for submetre accuracy. But in many regions like Australia there are no SBAS services for low-end users. As a result, many safety features of the imported vehicles that depend on SBAS signals will not function in Australia.

The explosive growth of another emerging application, unmanned aerial vehicles (UAV), has been reported recently: the Teal Group notes that the UAV market will reach $67.3 billion by 2024 (Huo Guang, 2016). In December 2013, Jeff Bezos, CEO of Amazon.com, announced on the “60 Minutes” show that drones could be used to speed the delivery of packages to consumers (Barr, 2013). Since

then, UAV for delivery has had much attention. But its commercialization remains stagnant. One of the reasons is that to make UAV well targeted, decimetre-level positioning will be required, otherwise an item would be as risk of falling into a pool while its configured destination refers to the garden one metre away from the pool. However, the cost of a UAV equipped with a high-end GPS can range from $10,000 to $100,000 (Rango et al., 2009; Xin, 2016), which is far from affordable.

Other new applications include entertainment and sports. Nowadays, it has become very important for hikers, tourists, runners, cyclists, or racing drivers to monitor their activities in terms of training features such as position, speed, landmarks or waypoints that can lead the user back to the initial position. In the future, more activities will be involved, such as concealing from or catching the enemy in paintball war game, or to jockey for position in basketball training. For their device performance, these sports people are interested in sub-metre to decimetre level accuracy, and in compact, low weight, and long battery-life units. This positioning ability targets the market of GNSS relative product not only for individuals, but also to a broader spectrum of users like business companies. For example, theme park administrators could manage attractions in a highly efficient way by analysing the visitors' distribution.

To sum up, the above applications have both concerns on economic efficiency and positioning performance (one-metre to decimetre precision). Generally, SF L1 GNSS receivers satisfy the budget, although their performance is inadequate. There is a gap between the current mass market and the professional market. This gap motivates research into improving SF GNSS receiver performance.

1.2 CONTEXT

The distances between satellites and a receiver, used in the receiver position computation, is measured by the time difference between a signal being transmitted from the satellite and being received by the receiver. These distance estimates are satisfactory provided that the satellite and the receiver clocks are synchronized and the signals always travel at the speed of light. However, this is never the case. During the propagation path, the signal may be delayed or advanced, leading to the biased ranges, thus positioning precision degradation. Many key factors limit the decimetre positioning capabilities with SF receivers, including satellite ephemeris and clock

errors, receiver clock and noise, atmosphere (ionosphere and troposphere) delay, and multipath interference.

Correction methods have already been developed for some of the above factors. Precise GNSS ephemeris and clock products have been provided by the international GNSS service (IGS) since 1994. This service provides GPS orbits with 3 – 5 cm accuracy, and satellite clocks at the sub-nanosecond level for users worldwide (http://igs.org/products). For the user segment, the receiver instrumental biases are commonly ignored, and can be absorbed during estimation. Elaborately designed receiver, for example narrowing the tracking loop bandwidth, allows minimization of the noise penalty (Braasch & Van Dierendonck, 1999). To account for tropospheric propagation effects, the Saastamoinen model is widely employed (Saastamoinen, 1972). Böhm, Black and Eisner have developed precise mapping functions for tropospheric correction (Black & Eisner, 1984; Böhm, Niell, Tregoning, & Schuh, 2006). Interference and multipath reduction can be achieved by proper antenna placement, elaborate antenna and advanced hardware design.

Among all error sources, the ionospheric effects are the ones that contributes the most, according to Tables 1.2 and 1.3 (Kaplan & Hegarty, 2005). It is also where the greatest difficulty lies. With the basic GNSS positioning mode, absolute positioning or single point positioning (SPP), the ionospheric delay is compensated by the Klobuchar model. Although SPP is very practical and cost-effective, the model can correct only 50% of the delay, achieving 4 m to 2 m positioning precision generally (Wu et al., 2013; Yuan et al., 2008). RTK, a type of relative positioning, is able to provide high precision at centimetre level because the ionospheric errors are mostly cancelled by double-differencing processing. However, RTK depends on the baseline length or density of nearby reference stations and it costs a lot (Wübbena et al., 2001). SBAS systems are designed to mitigate the ionospheric effects, offering 1 m to 2 m positioning services (Crespi *et al.*, 2012). Users in northern America and Europe, dependent on the coverage of Geostationary Earth Orbit (GEO) satellites, can be supported by SBAS services. But the services are not available in areas without GEO coverage such as Australia. Although some companies provide global services that cover Australia, for example Trimble RTX, they are commercial and require specific high-end receivers, which make the solution expensive (Chen et al., 2011). With dual-frequency (DF), the PPP algorithm precisely removes the

ionospheric delay with an ionosphere-free combination to achieve centimetre precision (Kouba *et al.*, 2001; Zumberge *et al.*, 1997), but a long convergence time is needed and the problem remains unsolved from when the PPP concept was first proposed. But it cannot be eliminated without DF signals. Therefore, ionospheric delay correction is the major challenge to SF receivers achieving decimetre-level positioning (Kaplan *et al.*, 2005). The performance and ionospheric correction strategy for current GNSS solutions are summarized in Table 1.4.

Table 1.2 Typical error budget of DF precise positioning services

Segment	Error source	1σ error (m)
Space/Control	Broadcast clock	1.1
	Broadcast ephemeris	0.8
User	Remaining ionospheric delay	0.1
	Remaining tropospheric delay	0.2
	Multipath	0.1
	Receiver noise	0.9
Total	Total	1.4

Table 1.3 Typical error budget of SF standard positioning services

Segment	Error source	1σ error (m)
Space/Control	Broadcast clock	1.1
	Differencial code bias	0.3
	Broadcast ephemeris	0.8
User	Ionospheric delay	> 7.0
	Tropospheric delay	0.2
	Multipath	0.1
	Receiver noise	0.3
total	Total	>7.1

Table 1.4 Current GNSS solution performance and their ionospheric correction strategies

Solution	Precision to be achieved	Ionospheric correction
SPS, PPS	Several metres	Klobuchar, Global Ionosphere Map (GIM)
SPP, SF-PPP, SBAS (WAAS, EGNOS, Trimble RTX)	Sub-metre to decimetre	GIM, Regional Ionosphere Map (RIM)
SF/DF-RTK, DF-PPP	Centimetre to millimetre	Network RTK, Ionosphere-free (IF)

Achieving higher accuracy requires data processing efforts at both the network end and the user end. At the network end, researchers and engineers make every effort to mitigate the errors through ionosphere modelling. However, the variations

of its spatial and temporal characteristics are very complicated, making it difficult to be precisely modelled. The Global Ionosphere Map (GIM) provided by International GPS Service (IGS) is one of the most popular ionospheric products. It is a 2.5°×5° grid map with 2-hour temporal resolution, based on a thin-layer assumption. It is generated from a global-scale reference network equipped with DF receivers. Currently, it is a combined product generated from four ionospheric associate analysis centres: Centre for Orbit Determination in Europe (CODE), Jet Propulsion Laboratory (JPL), European Space Agency (ESA) and Polytechnic University of Catalonia (UPC) (Feltens et al., 1998; Hernández-Pajares et al., 2009; Mannucci et al., 1998; Schaer et al., 1998).

However, ionospheric characteristics cannot be described accurately in large scale through a functional model. The corrections are not available for real-time applications, due to coarse temporal resolution and delayed update.

At the user end, GNSS receiver manufacturers may adopt advanced positioning algorithms. For example, the U-blox NEO-7P module provides precision better than one metre by combining the industry-proven PPP technology with SBAS, without the need for a reference station. However, mobile positioning and navigation software are barely improved. Assisted-GPS (A-GPS), the most popular solution for mobile phone users, requires specialized mobile software and hardware, and specialized servers (Van Diggelen et al., 2009). Through the Internet, additional information (precise ephemeris and clock, navigation message) are transmitted to mobile phones. At present, this method uses ionospheric correction inside the navigation message with the Klobuchar model only, by which the error cannot be mitigated very well. The A-GPS method aims to improve the signal receptions and the time to first fix. The common positioning precision is 10 metres (Zandbergen, 2009). Therefore, more studies need to be done with regard to SF receivers achieving sub-metre-precision demand in real-time applications.

In contrast to GIM, regional ionospheric maps (RIM) characterize vertical ionospheric delays over small regions with regional reference stations. The regional inter-station distance is shorter than the global reference station network on average, especially in areas like Australia and China (Li et al., 2014b). On one hand, with higher density regional-scale networks, RIMs are designed to offer better positioning accuracy than that can be supported by GIM. On the other hand, owing to its

adjustable temporal resolution, this method has the potential to be used for real-time applications. Regional ionosphere modelling is therefore the focus of this work.

1.3 OBJECTIVES

Within the context of Section 1.2, the major focus of this work is to explore the benefits of regional ionospheric corrections on SF GNSS receiver performance. The research focuses on the network end, user end, and experimental aspects.

From the perspective of the server end, RIM generation is the most critical issue. Common relevant information regarding ionosphere includes three aspects that need investigation: its frequency constraints, temporal-spatial constraints, and an *a priori* model. Especially for the temporal-spatial constraint, the mathematical function to represent the ionospheric temporal-spatial variation, evident difference exists between GIM and RIM. The spherical harmonic function and the polynomial function that are widely employed for GIM can be expected to perform well only when hundreds of reference stations are established. In addition, the function order is relevant to observing span (Li et al., 2012). Studying this problem should lead to a more general method that is applicable to single station data processing, rather than to reference station networks.

At the user end, importance should be attached to how to take advantage of the ready-to-use ionosphere corrections. New methodology and data formats needs to be established. Then new algorithms and software requires to be developed. These aims could be accomplished by modifying the positioning algorithms on the existing software platform RTKLIB, which is an open source program package for GNSS positioning. After investigation, the modified software should have the capability to deal with regional ionospheric corrections with station-based format.

In the study, we focus on the validation through experiments. The study is broken into two stages. In the first stage, downloaded GNSS raw measurements require to be processed and analysed. In the second stage, we aim to conduct real-time experiments, particular to road scenarios. The final objective is to verify that SF GNSS receivers are able to achieve decimetre positioning precision via regional ionospheric corrections.

1.4 SIGNIFICANCE AND OUTCOMES

By addressing the ionospheric relevant problems detailed in Section 1.3, this thesis makes the following four contributions: three technical outcomes and one outcome for GNSS markets.

At the server end, a new Australian regional ionospheric map is developed for GNSS positioning performance improvement. For its generation, this thesis adopts a new methodology, providing the station-based ionospheric map (SIM) along with the RIM generation, independent of the number of reference stations. Its station-based feature provides a flexible way for data transmission, making it possible to broadcast corrections from only a few surrounding stations. Therefore, the network traffic load can be alleviated. In order to apply this new form of corrections, the methods of data link and their standards are reviewed. Additionally, this station-based feature is able to exclude data of bad quality, making quality detection easier. As for the map quality, a high ionospheric temporal-spatial resolution is obtained. As a result, it has the potential to improve the GNSS positioning performance.

At the user end, new software is developed based on RTKLIB, enabling SPP and SP-PPP computation with the new ionospheric correction data format. Since corrections from only a few surrounding stations are received, the station-based strategy relies on the availability but not very much on the capacity of the data link, which gives cost-efficiency. In addition, the strategy for each error source correction is studied in detail. Generally, this study develops an aspiring approach for improving positioning accuracy at the user end. It can be further developed with multi-constellation, and combined with inertial navigation system (INS), to achieve better performance.

Thirdly, an overall data processing idea called coordinate space representation (CSR) is proposed. With this method, the correction is conducted in the position domain. Its core idea is that coordinate corrections of one station can help its surrounding stations improve their coordinate precision. The obvious advantage over other differencing techniques is its independence of raw data at either the server end or at the user end. Therefore, it can be regarded as a lightweight mechanism.

From the application aspect, the quantity of GNSS devices in use is forecasted to be over 7 billion by 2019, an average of one device per person on the planet. Such

a mass market has been and will continue to be dominated by low-end positioning devices like smartphones. For their poor positioning performance, currently smartphones are mostly applied to LBS, which has a accuracy requirement of tens-of-metres; they are not able to realise higher demand mass-market applications such as intelligent transport systems (ITS) and GIS. With the contributions of this thesis, significant enhancement can be made on the positioning precision of SF GNSS devices. Even low-cost GNSS boards used in smartphones have the potential for submetre applications. Therefore, all the applications elaborated in Section 1.1, including all lane-level traffic applications, accurate data collection, accurate delivery with UAV, and even many sport and recreation applications can be realised. Meanwhile, remarkable economic benefits could be achieved.

1.5 THESIS OUTLINE

Section 2 reviews the literature related to the research problem in this thesis. In this section, a basic mathematic model is first introduced. Different GNSS services and computation modes are then outlined, in terms of definition, of how they deal with errors, and of their pros and cons. In particular, ionospheric modelling approaches for various modes are reviewed.

Section 3 provides the methodological analysis of ionospheric correction generation. At the user end, various error sources that affect decimetre or higher precision are examined, including precise orbits and clocks, differential code bias, solid earth tide, phase centre offset and windup. A CSR method is proposed here to provide an easy approach for low-cost receivers to improve positioning precision, based on the time tag and their navigation solution.

Section 4 presents the experimental results: ionospheric map quality; interpolated station-based ionosphere model (SIM) performance; kinematic positioning performance with high-end receivers; dynamic positioning with low-cost receiver; and the usage of ionospheric map on CSR solution. Analyses demonstrate how ionosphere delay corrections from 200 stations in Australia can support SF SPP and PPP for decimetre solutions.

Section 5 summarises the research and significance presented in this thesis and emphasises the contribution and outcomes.

Chapter 2: A review of GNSS positioning modes and ionosphere modelling

This chapter reviews known error correction techniques and provides arguments to support the study focus. It starts with a review of the basic observation equations in Section 2.1. Then the existing GNSS computation modes are synthesized and integrated in Sections 2.2 and 2.3. Section 2.4 critically evaluates the literature of the ionospheric correction methods. Standards of data links are discussed in Section 2.5.

2.1 BASIC EQUATIONS

Every GPS application ultimately involves the determination of platform position, velocity, or time. The exact algorithms and implementations may differ depending on the application. But in each case the most fundamental ideas remain the same: to obtain the precise user-to-satellite line-of-sight (LOS) distance. The original measurements including observables and navigation messages are transmitted to users in the form of binary data via a spread-spectrum communication technique (Proakis, 2001). The range, received in terms of propagation time and then multiplied by the speed of light, is regarded as pseudorange instead of real range, because the receiver time bias can be very large due to the local clocks. For a DF GPS receiver, each set of signals consists of three code components — C1 (C/A code modulated on L1 frequency), P1 (P code modulated on L1 frequency), and P2 (P code modulated on L2 frequency) — and two carrier phase components — L1 and L2. The measurements can be presented as the following observation equations in terms of range in meters (Rho *et al.*, 2007):

$$
\begin{aligned}
C_1 &= \rho - c \cdot t^s + c \cdot t_r + T + I - b^s_{C1-ref} + b^r_{C1-ref} + e_{C_1} \\
P_1 &= \rho - c \cdot t^s + c \cdot t_r + T + I - b^s_{P1-ref} + b^r_{P1-ref} + e_{P_1} \\
P_2 &= \rho - c \cdot t^s + c \cdot t_r + T + \gamma I - b^s_{P2-ref} + b^r_{P2-ref} + e_{P_2} \\
L_1 &= \rho - c \cdot t^s + c \cdot t_r + T - I - \lambda_1 \cdot N_1 + \Delta\emptyset + e_{L_1} \\
L_2 &= \rho - c \cdot t^s + c \cdot t_r + T - \gamma I - \lambda_2 \cdot N_2 + \Delta\emptyset + e_{L_2}
\end{aligned}
\qquad (2.1)
$$

where the subscripts “1” and “2” refer to frequency L1 and L2; c is the speed of light; t^s and t_r indicate satellite and receiver clock errors; T and I are troposphere and ionosphere delays; b^s and b_r stand for satellite code bias and receiver instrumental bias; e represents other errors such as multipath, receiver noise, and antenna phase centre offset (Misra & Enge, 2006). For carrier phase equations, λ is carrier wave length; N includes the carrier phase ambiguity and the satellite and receiver instrumental phase delays; $\Delta\emptyset$ is the phase windup error; and ρ denotes the geometric distance between satellite $r^s(x^s, y^s, z^s)$ and receiver $r_r(x_r, y_r, z_r)$:

$$\rho = \sqrt{(x^s - x_r)^2 + (y^s - y_r)^2 + (z^s - z_r)^2} \tag{2.2}$$

The above equations must be linearised in order to estimate the user states. In the linearisation process, all the computed or known terms are moved to the left-hand side.

$$\begin{aligned}
dC_1 &\equiv C_1 - \hat{\rho} + c \cdot t^s - T_0 - I_0 + b^s_{C1-ref} = \boldsymbol{H_s \delta x} + dT + dI + b^r_{C1-ref} + e_{C_1} \\
dP_1 &\equiv P_1 - \hat{\rho} + c \cdot t^s - T_0 - I_0 + b^s_{P1-ref} = \boldsymbol{H_s \delta x} + dT + dI + b^r_{P1-ref} + e_{P_1} \\
dP_2 &\equiv P_2 - \hat{\rho} + c \cdot t^s - T_0 - \gamma I_0 + b^s_{P2-ref} = \boldsymbol{H_s \delta x} + dT + \gamma dI + b^r_{P2-ref} + e_{P_2} \\
dL_1 &\equiv L_1 - \hat{\rho} + c \cdot t^s - T_0 + I_0 - \Delta\emptyset = \boldsymbol{H_s \delta x} + dT - dI - \lambda_1 \cdot N_1 + e_{L_1} \\
dL_2 &\equiv L_2 - \hat{\rho} + c \cdot t^s - T_0 + \gamma I_0 - \Delta\emptyset = \boldsymbol{H_s \delta x} + dT - \gamma dI - \lambda_2 \cdot N_2 + e_{L_2}
\end{aligned} \tag{2.3}$$

Corrections should be applied consistently. For example, code biases are highly correlated to the satellite clock. It comes from IGS when IGS precise ephemeris and clock products are applied; or from the navigation message when the broadcast ephemeris is used. The known parts include:

- $\hat{\rho}$: the approximate range computed by the satellite coordinate $r^s(x^s, y^s, z^s)$, the approximate rover coordinate $\hat{r}_r(\hat{x}_r, \hat{y}_r, \hat{z}_r)$, and the approximate clock bias $\hat{t}_r$. Symbol ^ denotes an approximate value that is iterated repeatedly. Satellite coordinate can be obtained from broadcast navigation message or the IGS precise products:

$$\hat{\rho} = \sqrt{(x^s - \hat{x}_r)^2 + (y^s - \hat{y}_r)^2 + (z^s - \hat{z}_r)^2} + c \cdot \hat{t}_r \tag{2.4}$$

- t^s : satellite clock error correction that can be retrieved from its broadcast navigation message or the IGS precise products;
- T_0 : tropospheric delay correction either estimated or computed by the Saastamoinen model and the Niell or the Black and Eisner mapping functions;
- I_0 : ionospheric delay correction either estimated or derived from the broadcast navigation message, the global or regional ionospheric map, or slant corrections;
- $b^s_{obs-ref}$: satellite Differential Code Biases (DCB), where "obs" refers to the observation being used and "ref" denotes the reference for a correction.

The unknown parts are:

- $\boldsymbol{H_s}$: the design matrix that is computed by the partial derivatives of each observable with respect to each unknown parameter;

$$\boldsymbol{H_s} = \left[\frac{-(X^s - x)}{\rho} \quad \frac{-(Y^s - y)}{\rho} \quad \frac{-(Z^s - z)}{\rho} \quad 1\right]_{\boldsymbol{\rho=\hat{\rho}}} \tag{2.5}$$

- $\boldsymbol{\delta x} = (\Delta x, \Delta y, \Delta z, c\Delta t_r + b^r_{obs-ref})$: increment of the unknown receiver location and clock bias to the coarse initial part;
- dT, dI : residual tropospheric and ionospheric bias that cannot be mitigated by models;
- $b^r_{obs-ref}$: receiver instrumental group delay that is usually absorbed by the receiver clock; "obs" and "ref" denotes the same meaning as satellite DCB;
- N : carrier phase ambiguity. Phase instrumental delays are assimilated in it, and are estimated as floating ambiguities when in precise positioning mode;
- e : multipath and receiver noise.

In terms of matrices and vectors, the linear equation for each type of pseudorange measurement in (2.3) can be represented as:

$$d\boldsymbol{P} = \boldsymbol{H\delta x} + \boldsymbol{e} \tag{2.6}$$

For each type of carrier-phase equation in (2.3), the linear equation is expressed as

$$dL = \boldsymbol{H\delta x} + \boldsymbol{\lambda N} + \boldsymbol{\varepsilon} \tag{2.7}$$

In (2.6) and (2.7), d$\boldsymbol{P}$ represents the residual vector for all the code measurements $C_1, P_1, or\ P_2$ at receiver "r"; $d\boldsymbol{L}$ represents the residual vector for all the phase measurements $L_1,\ L_2$ at receiver "r". $\boldsymbol{H}$ is the design matrix that contains the linear coefficients; $\boldsymbol{\delta x}$ denotes the unknown vector to be estimated; N is the real value ambiguity vector that containing the phase instrument biases; $\boldsymbol{e}$ is the code measurement error vector; and ε is the phase measurement error vector.

The statistical models for the linear equations (2.6) and (2.7) are their expectation vectors and covariance matrices of the error vectors, which are expressed as:

$$E(\boldsymbol{e}) = 0\,, \quad E(\varepsilon) = 0\,, \tag{2.8}$$

$$Cov(\boldsymbol{e}) = E(\boldsymbol{e} \cdot \boldsymbol{e}^T) = \sigma_P^2 \boldsymbol{R}, \quad Cov(\boldsymbol{\varepsilon}) = E(\boldsymbol{\varepsilon} \cdot \boldsymbol{\varepsilon}^T) = \sigma_L^2 \boldsymbol{Q} \tag{2.9}$$

where $\boldsymbol{R}$ and $\boldsymbol{Q}$ are the co-factor variance matrices related to measurement error vectors **e** and $\boldsymbol{\varepsilon}$, respectively; σ_P^2 and σ_l^2 are the variance of the user range error that contains errors of each segment. They are computed as:

$$\sigma_{\mathrm{P}}^2 = \sigma_{orb}^2 + \sigma_{clk}^2 + \sigma_{T0}^2 + \sigma_{I0}^2 + \sigma_{mp}^2 + \sigma_p^2 \tag{2.10}$$

$$\sigma_L^2 = \sigma_{orb}^2 + \sigma_{clk}^2 + \sigma_{T0}^2 + \sigma_{I0}^2 + \sigma_{ml}^2 + \sigma_l^2 \tag{2.11}$$

where σ_{orb} and σ_{clk} represents the standard deviation of the effects of satellite orbit and clock errors on the computed range; σ_{T0} is the standard deviation of the troposphere delay error after correction with an empirical model; σ_{I0} is the standard deviation of the ionosphere error after corrections; σ_{mp} and σ_{ml} are the standard deviations of the code and phase multipath errors, respectively; $\sigma_p$and σ_l are the standard deviations of the receive code and phase noises. The total variances σ_{P}^2 and σ_{l}^2 also generally depend on how the co-factor matrices R and Q are structured and combined. The size of each component will be discussed in each positioning mode.

After solving the four unknown increments, the approximate values are updated as follows:

$$\begin{cases} x_r = \hat{x}_r + \Delta x \\ y_r = \hat{y}_r + \Delta y \\ z_r = \hat{z}_r + \Delta z \\ ct_r = c\hat{t}_r + c\Delta t_r + b^r_{obs-ref} \end{cases} \tag{2.12}$$

Iterations are conducted by repeating this procedure until the increments reach a prescribed threshold.

In the following sections, we focus on five different positioning modes.

2.2 GNSS COMPUTATION MODES

Various GNSS computing modes apply different strategies to deal with the unknowns, biases and noise terms under certain conditions. In this section, five basic GNSS positioning modes are discussed from the perspectives of definition, algorithm, how they deal with the biases and errors, and the pros and cons: single point positioning (SPP), differential GNSS (DGNSS), satellite-based augmentation system (SBAS), real-time kinematic (RTK), and precise point positioning (PPP). This discussion provides the basis for the research focus of this thesis.

2.2.1 Single Point Positioning (SPP)

Single point positioning or absolute positioning is defined as a single receiver positioning in a coordinate system whose origin is uniquely defined (Rizos, 1997). In the most widely applied case, satellite coordinates and clocks are given by broadcast navigation messages; ionospheric delay corrections are retrieved from the navigation messages as well; tropospheric delay corrections are computed from empirical models such as the Saastamoinen model. Other secondary error sources are usually ignored, including satellite and receiver signal delay (such as DCB), satellite antenna offset, and the site displacement effect. Figure 2.1 depicts a typical SPP system.

In the case of a single GNSS system, usually more than four satellites are observed at the same time. While vector $\boldsymbol{\delta x}$ in equation (2.6) contains four parameters, all of the matrices contain more than four measurements. Therefore, the least square (LS) method is applied to solve the vector $\boldsymbol{\delta x}$.

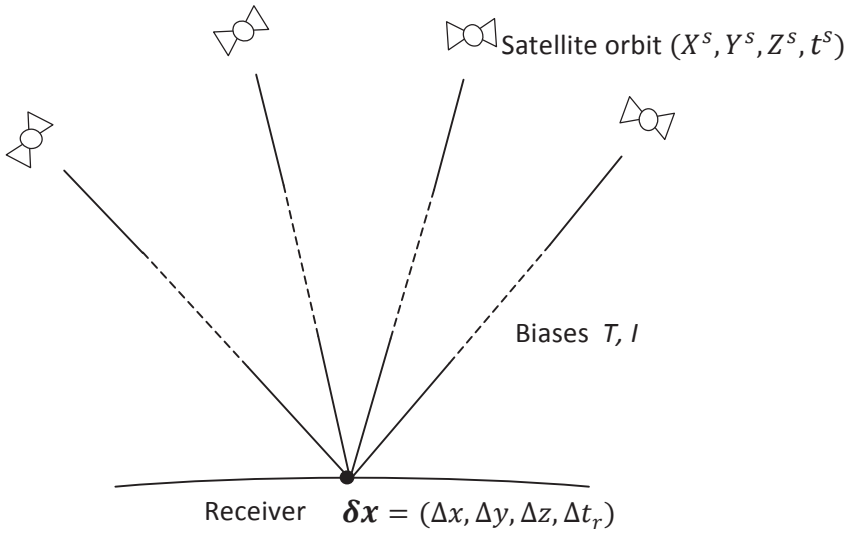

Figure 2.1 SPP computation mode

The LS solutions can be achieved by computing the partial derivative of $\|d\boldsymbol{P} - \boldsymbol{H\delta x}\|^2$ with respect to $\boldsymbol{\delta x}$:

$$\frac{d}{d(\boldsymbol{\delta x})}\|d\boldsymbol{P} - \boldsymbol{H\delta x}\|^2 = 2\boldsymbol{H}^T\boldsymbol{H\delta x} - 2\boldsymbol{H}^T d\boldsymbol{P} = \boldsymbol{0} \tag{2.13}$$

The unknowns are solved as:

$$\boldsymbol{\delta\hat{x}} = (\boldsymbol{H}^T\boldsymbol{H})^{-\boldsymbol{1}}\boldsymbol{H}^T d\boldsymbol{P} \tag{2.14}$$

Furthermore, since the measurement error is different for satellites, a weight can be set for each satellite. The larger the weight, the more important role the measurement will play in the LS procedure. This is the weighted least square (WLS) method. By introducing the measurement covariance matrix $\boldsymbol{R}$, $\boldsymbol{\delta x}$ is solved as:

$$\boldsymbol{\delta\hat{x}} = (\boldsymbol{H}^T\boldsymbol{R}^{-1}\boldsymbol{H})^{-\boldsymbol{1}}\boldsymbol{H}^T\boldsymbol{R}^{-1}d\boldsymbol{P} \tag{2.15}$$

and its covariance matrix is

$$Cov(\boldsymbol{\delta\hat{x}}) = E(\boldsymbol{\delta x}\cdot\boldsymbol{\delta x}^T) = \sigma_P^2(\boldsymbol{H}^T\boldsymbol{R}^{-1}\boldsymbol{H})^{-\boldsymbol{1}} \tag{2.16}$$

If the code measurement errors have independent and identically distributed (i.i.d) variances, their covariance matrix $Cov(\boldsymbol{e})$ and the covariance matrix of positioning error $Cov(\boldsymbol{\delta x})$ are expressed as:

$$Cov(\boldsymbol{e}) = \boldsymbol{\sigma_P^2 I} \tag{2.17}$$

$$Cov(\boldsymbol{\delta\hat{x}}) = \sigma_P^2(\boldsymbol{H}^T\boldsymbol{H})^{-\boldsymbol{1}} \tag{2.18}$$

where $\boldsymbol{I}$ is a unit matrix. Equation (2.18) follows from (2.16) if $\boldsymbol{R} = \boldsymbol{I}$.The inverse matrix $(\boldsymbol{H}^T\boldsymbol{H})^{-1}$ also defines the various dilution of precision (DOP) values for assessment of the geometric impact of the system on the SPP solution.

The LS solution (2.14) or the WLS solution (2.15) is the most basic GNSS positioning solutions. The accuracy of the SPP solution depends on three factors: the total standard deviation σ_P, the design matrix $\boldsymbol{H}$ that is related to the satellite geometry, and the co-factor matrix $\boldsymbol{R}$ or the setting of the weight matrix $\boldsymbol{R}^{-1}$. $\boldsymbol{R} = \boldsymbol{I}$ is one of the weigh matrix settings. In addition, the SPP solution has not involved phase measurements (2.7). Tables 1.2 and 1.3 show the user range errors for SPP solutions with DF or SF code measurements. More positioning modes have been developed to address one or more factors in order to improve the positioning solutions. Code-based differential GNSS reduces the error components that contributed to σ_P as shown in (2.6). Multiple GNSS systems use more satellites in view to improve the satellite geometry. SBAS makes use the precise orbit, clock and ionosphere corrections; and RTK and PPP introduce precise phase measurements and reduce the effects of various errors. With IGS ionospheric products, the positioning accuracy can be further improved to 1.5 m in mid-latitude areas (Minkwitz, Gerzen, Wilken, & Jakowski, 2014; Øvstedal, 2002; Satirapod, Rizos, & Wang, 2001).

2.2.2 Differential GNSS (DGNSS)

Differential or relative positioning refers to determination of a user receiver's coordinates relative to a "reference receiver" with precise known coordinates (Parkinson & Enge, 1996). The reference station is designed to deliver information to the user via a satellite or terrestrial data link. The information contains:

- Observables at reference stations (pseudorange or carrier phase);
- Measurement corrections for user receiver, and substitute for broadcast satellite orbit and clock;
- Integration information;
- Auxiliary data, including station coordinate, health status, and meteorologic data.

Differential GNSS uses the single-differenced (SD) code measurements between the reference station and the user receiver for the same satellites. Forming

single difference (SD) eliminates the common errors of two receivers. Figure 2.2 depicts a typical DGNSS system.

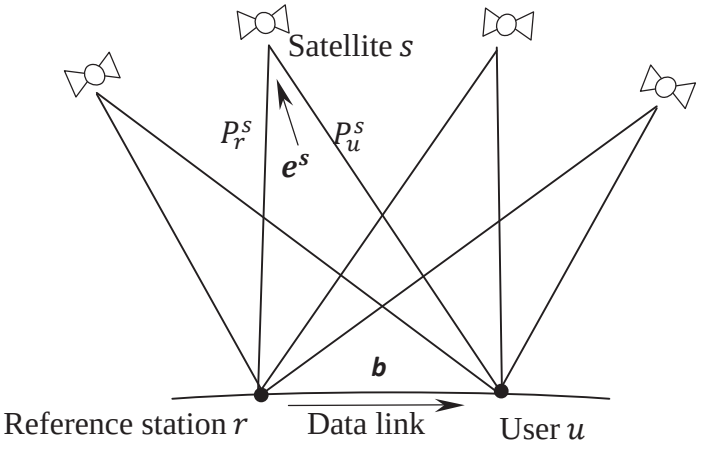

Figure 2.2 DGNSS system

As shown in Figure 2.2, the SD between receiver u and r for the satellite s is formed as:

$$\Delta P_{ur}^s = P_u^s - P_r^s$$

$$= \left(\rho_u^s - ct^s + ct_u + T_u^s + I_u^s + e_k^p\right) - (\rho_r^s - ct^s + ct_r + T_r^s + I_r^s + e_r^s)$$

$$= \rho_u^s - \rho_r^s + ct_{ur} + [T_u^s - T_r^s] + [I_u^s - I_r^s] + e_{ur}^s \quad (2.19)$$

where the subscripts "r" and "u" represent reference and user receiver respectively and the superscript "s" represents satellite s. After differencing, the linear equation for the SD measurements is formed as:

$$\Delta dP_{ur}^s = dP_u^s - dP_r^s = P_u^s - P_r^s - (\hat{\rho}_u^s - \hat{\rho}_r^s) - [T_{u0}^s - T_{r0}^s] - [I_{u0}^s - I_{r0}^s] +$$
$$= \boldsymbol{H_s dx} + dT_{ur} + dI_{ur} + db_{Obs-ref}^{ur} + de_{ur}^s \quad (2.20)$$

If the coordinates of the reference receiver are treated as knowns, the state coordinate biases are defined with respect to the reference receiver$\boldsymbol{dx} = (\Delta x, \Delta y, \Delta z, c\Delta t_{ur} + db_{obs-ref}^r)$. Evidently, the common error sources for both receivers, including the satellite clock offset, DCB, and ephemeris, and atmosphere effect dT and dI, are cancelled completely or to a great extent. The residual errors that directly influence the DGNSS performance are outlined as follows:

- Satellite orbit error residuals: these are proportional to the baseline length. For a 100 km baseline above 5° elevation, the correction error is less than 2.5 cm, assuming that the orbit error is 5 m;
- Tropospheric delay residuals: for a 100 km baseline at a 45° elevation, the values show a difference of 9 mm between the reference station and user;
- Ionospheric delay residuals: they vary with elevation angle and baseline length. For a 100 km baseline at a 45° elevation in temperate regions, the ionospheric correction difference is around 3 cm;
- Multipath and receiver noise: these are not proportional to either baseline or elevation. The effects on both reference and user receivers are included. This may be the dominant source of the errors.

For a short baseline (< 100km), multipath is the biggest error source. But for a long baseline, the residual ionospheric delays could be non-negligible. The spatial variation of ionosphere plays a more important role than the elevation angle. The vertical ionosphere delays caused by total electron content (TEC) gradient reach 0.5 m without and over 4 m with ionospheric disturbance at a 100 km baseline (Komjathy, Sparks, Mannucci, & Coster, 2005; Wanninger, 1993).

2.2.3 Satellite Based Augmentation System (SBAS)

SBAS is an extension of the wide area differential GPS (WADGPS) concept (Kee, Parkinson, & Axelrad, 1991). With continuously operating reference stations (CORS) and main control station (MCS) as its ground facilities, pseudorange and carrier phase measurements are collected from the whole ground network, processed at MCS and uploaded to a geostationary satellite. With GEO satellites as the data communication link, the system provides satellite clock and ephemeris corrections, real-time ionospheric corrections, along with integrity information (Figure 2.2). The GEO satellites also provide GPS-like range signals at L1 signals.

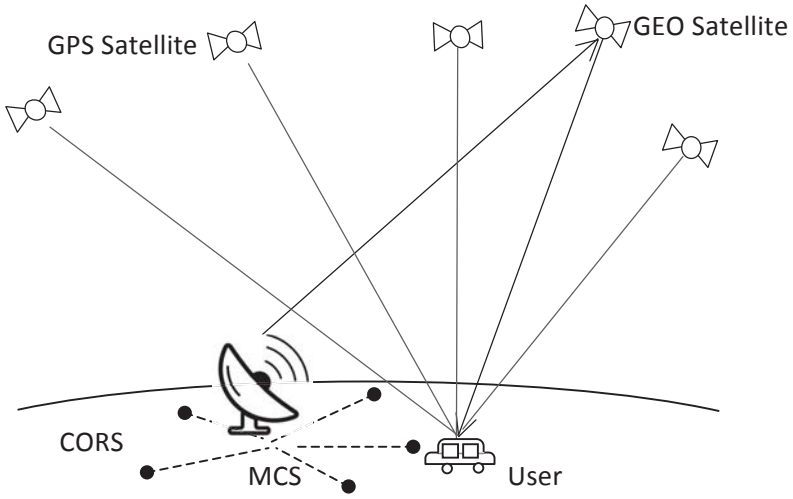

Figure 2.3 SBAS structure

Rather than depending on the pseudorange corrections from a nearby station, the system deals with the major error sources in a centralised way, and computes them for a region. Therefore, the user positioning performance is independent of its distance to the surrounding stations. SBAS is designed to offer 1 to 2 metres of precision performance for SF L1 users (Crespi *et al.*, 2012). It is code-based because the user end strategy is based on pseudorange — corrections are directly added to the C/A or the P1 code:

$$\Delta C_1 \equiv C_1 - \hat{\rho} + c \cdot t^s - T_0 - \left(d\rho_{eph} - dt_{eph} + I_{sbas}\right) = \boldsymbol{H\delta x} + dT + e_{C_1}$$

$$\Delta P_1 \equiv P_1 - \hat{\rho} + c \cdot t^s - T_0 - \left(d\rho_{eph} - dt_{eph} + I_{sbas}\right) = \boldsymbol{H\delta x} + dT + e_{P_1} \quad (2.21)$$

- $\hat{\rho}$ and clock t^s are computed with the satellite orbit $r^s(x^s, y^s, z^s)$ from the broadcast ephemerides, and the range correction term $d\rho_{eph}$ is derived from the SBAS messages with respect to the broadcast messages.
- The tropospheric delay correction T_0 is computed from model and directly added to the measurement;
- The ionospheric delay corrections I_{sbas} are obtained from those SBAS messages that include a vertical grid map. Users do interpolation among the grid points and map the values to slant direction, then add them to the pseudorange;

- Multipath, receiver noise along with the residual tropospheric error *e* is computed according to elevation angles and formed into a holistic pseudorange residual.

Figure 2.3 illustrates the coverage of the existing SBASs, involving American WAAS, European EGNOS, Japanese MSAS, and others (EL - ARINI et al., 1994; Kaplan *et al.*, 2005). These services are free but do not cover Australia. Due to channel capacity, their satellite-based characteristics limit the resolution of ionospheric grid maps, which results in the limitation of the positioning precision improvement. Although some companies, such as Trimble, provide global services that cover Australia, they are commercial and require specified receivers, which make the solution expensive (Chen et al., 2011).

Figure 2.4 Coverage of the existing SBAS

2.2.4 Real Time Kinematic (RTK)

Based on the carrier phase observables along with the pseudorange, centimetre-level positioning performance has been made available with very short observation time at the user end. This technique is called real-time kinematic (RTK). Since the carrier phase introduced integer ambiguity, ambiguity resolution (AR) has become the biggest difficulty. The system complexity and cost have increased (Rizos, 2009; Wübbena et al., 2001).

The method RTK uses to deal with errors is observation space representation (OSR), by which the sum of error components is represented in observation space. By applying double-differencing (DD) technique to the code and carrier phase observables, the majority of error sources is cancelled. Double differences can be obtained by differencing two single differences from two satellites. Figure 2.4 depicts a typical DD relationship consisting of two satellite and two receivers. Since

the baseline, or in other words the reference-to-user distance, is much shorter than the satellite height, the propagation paths from the same satellite can be regarded as parallel.

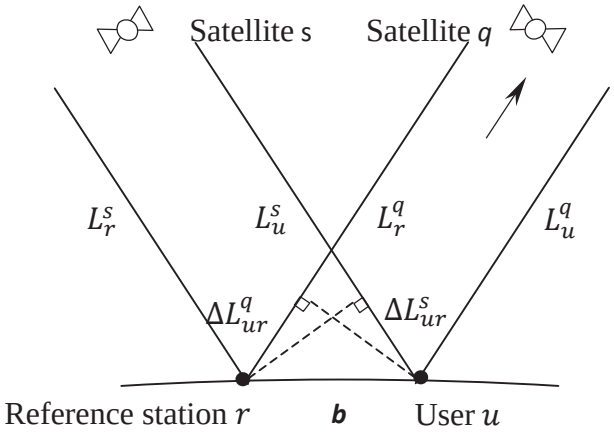

Figure 2.5 Typical DD relationship

As for the single-differencing (SD) operation for code measurements, the SD for the phase measurements between receiver u and r for the satellite s is formed as:

$$\Delta L_{ur}^s = L_u^s - L_r^s$$

$$= (\rho_u^s - ct^s + ct_u + T_u^s - \lambda N_u^s - \varepsilon_u^s) - (\rho_r^s - ct^s + ct_r + T_r^s - I_r^s - \lambda N_r^s - \varepsilon_r^s)$$

$$= \rho_u^s - \rho_r^s + ct_{ur} + (T_u^s - T_r^s) + (I_u^s - I_r^s) - \lambda N_{ur}^s + \varepsilon_{ur}^s \quad (2.22)$$

The DD operation takes the difference between two SDs. On its formation, receiver clock errors are eliminated completely. Over the short inter-receiver distances, the effects of residual troposphere and ionosphere delays are eliminated. The DD code and phase measurements are formed as follows

$$\nabla\Delta P_{ur}^{sq} = \Delta L_{ur}^s - \Delta L_{ur}^q = \rho_u^s - \rho_r^s - (\rho_u^q - \rho_r^q) + e_{ur}^{sq} \quad (2.23)$$

$$\nabla\Delta L_{ur}^{sq} = \Delta L_{ur}^s - \Delta L_{ur}^q = \rho_u^s - \rho_r^s - (\rho_u^q - \rho_r^q) + \lambda N_{ur}^{sq} + \varepsilon_{ur}^{sq} \quad (2.24)$$

The hardware biases in the ambiguity term *N* are also cancelled in the DD processing. With both DD code and the phase equations (2.23) and (2.4), the DD integer ambiguity term N_{ur}^{sq} can be resolved through the approach such as integer least square. After the integer N_{ur}^{sq} is correctly fixed and kept known, the equation (2.24) can then be used for precise position estimation.

2.2.5 Precise Point Positioning (PPP)

The concept of PPP was first introduced by Zumberge (Zumberge et al., 1997). To achieve precise positioning, it requires the knowledge of all error components with a good accuracy. Unlike SPP or DGNSS, the effects of troposphere error are treated as parameters of the state vector to be estimated in PPP, independent of reference stations. PPP may use different combinations of code and phase measurements. In the most representative DF-PPP mode, the ionosphere-free (IF) combinations are formed to eliminate the ionospheric delay in both code and phase measurements.

$$P_{IF} = \alpha C1 - \beta P2$$

$$= \left(\rho - c \cdot t^s + c \cdot t_r + T - \left[\alpha b^s_{C1-ref} - \beta b^s_{P1-ref}\right)\right] + e_{P_{IF}} \quad (2.25)$$

$$L_{IF} = \alpha L1 - \beta L2 = (\rho - c \cdot t^s + c \cdot t_r + T - \lambda_{IF} N_{IF} + \Delta\emptyset + \varepsilon_{L_{IF}} \quad (2.26)$$

where α and β are coefficients related to frequencies f_1 and f_2,

$$\alpha = \frac{f_1^2}{f_1^2 + f_2^2}, \qquad \beta = \frac{-f_2^2}{f_1^2 + f_2^2}, \qquad \lambda_{IF} = \alpha\lambda_1 - \beta\lambda_2 \quad (2.27)$$

For PPP, it is assumed that the satellite orbit (X^s, Y^s, Z^s) and clock t^s will use precise orbit and clock products, such as the IGS ultra-rapid orbit products, instead of the broadcast message. Satellite DCB b^s is also obtained from IGS product.

Then linearisation of the IF observation equations (2.25) and (2.26) becomes:

$$\begin{bmatrix} \boldsymbol{dP}_{IF} \\ \boldsymbol{dL_{IF}} \end{bmatrix} = \boldsymbol{H_{IF}}\boldsymbol{\delta x} + \boldsymbol{e} \quad (2.28)$$

where dP_{IF} is the vector of residuals, $\boldsymbol{H}$ is the design matrix, $\boldsymbol{\delta x}$ is the vector of corrections to the unknown parameters, $\boldsymbol{e}$ is the measurement error. For PPP mode, the estimated vector consists of three more types: troposphere zenith path delay zpd, and non-integer carrier phase ambiguities N, and the user receiver DCB parameter:

$$\boldsymbol{\delta x} = \begin{bmatrix} \Delta x \\ \Delta y \\ \Delta z \\ \Delta t_r \\ \Delta zpd \\ \Delta N \\ b_{IF} \end{bmatrix} \quad (2.29)$$

$$\boldsymbol{H_{IF}} = \begin{bmatrix} \frac{\partial \rho}{\partial x} & \frac{\partial \rho}{\partial y} & \frac{\partial \rho}{\partial z} & 1 & \frac{\partial T}{\partial zpd} & 0 & 1 \\ \frac{\partial \rho}{\partial x} & \frac{\partial \rho}{\partial y} & \frac{\partial \rho}{\partial z} & 1 & \frac{\partial T}{\partial zpd} & -\lambda_{IF} & 0 \end{bmatrix} \tag{2.30}$$

All the other error sources that are usually ignored by other positioning modes should be taken into consideration here, including satellite antenna offset, phase wind-up, and earth tide load. In addition, it is necessary to estimate the bias of the pseudorange and carrier phase observables for each satellite.

Theoretically, with combined DF observables and precise satellite orbit and clock products, PPP can achieve cm-level 3D position accuracy after convergence. A significant problem for PPP is the convergence time, which is usually tens of minutes to hours. A PPP user requires only a single GNSS receiver; therefore, no reference stations are needed surrounding the user although the orbits and clocks are determined with a global network. Another attraction of PPP is that it supports applications other than positioning, for example, troposphere estimation, ionosphere estimation, and crustal deformation monitoring. When a regional network of stations is available, the PPP with ambiguity resolution (PPP-AR) can be used instead to achieve faster convergence and more precise positioning solutions (Collins, 2008).

PPP and PPP-AR suffer from several weaknesses. PPP usually uses a high-end DF receiver; thus some researchers have explored SF-PPP. Yet for SF receivers, external ionosphere information such as a vertical TEC map or a slant TEC correction is a necessity (Li *et al.*, 2014b; Shi *et al.*, 2012). On the other hand, convergence time is a bottleneck. After new observables are calculated, a Kalman filter is utilised in iterative error estimation and to resolve ambiguity, which usually takes tens of minutes. Recent studies show that convergence time can be improved to several minutes (Banville *et al.*, 2014; Hongping Zhang *et al.*, 2013).

2.3 SUMMARY OF POSITIONING MODE

Overall, the GNSS computing modes and how they treat the parameters are summarised in Table 2.2. Different modes have different pros and cons. Among those, SPP is the most cost-effective while SP-PPP is able to achieve higher precision than SPP. This study therefore focuses on sub-metre to decimetre positioning performance with both SPP and SF-PPP computation modes.

Table 2.1 GNSS computing modes VS treatment of parameters. C=Cancelled; E= Estimated; G= Given; N/A=Not Available

Positioning mode	SPP	DGNSS	SBAS	RTK	PPP
Measurement type	C1, P1, P2	C1, P1, P2	C1, or P1	P1, P2 L1, L2	C1, P1, P2, L1,L2
Satellite position r^s	G	G	G	G	G
receiver position r_r	E	E	E	E	E
Satellite clock t^s	G	C	G	C	G
Receiver clock t_r	E	C	C	C	E
Tropospheric delay T	G	C	C	E	E
Ionospheric delay I	G / C	C	G	E	C / E
Instrumental code delay b^s_{code}	G	C	G / C	C	G / E
Instrumental phase delay b^s_{phase}	N/A	N/A	N/A	C	E
Ambiguity N	N/A	N/A	N/A	E	E
Stochastic error e	G	G	G	G	G

2.4 IONOSPHERE-MODELLING APPROACHES FOR VARIOUS MODES

Among many error sources, the ionosphere delay is the major challenge for SF receivers achieving decimetre precision. The SPP and SF-PPP modes can only perform well when this delay is eliminated. Alas, the form and variation of ionosphere are subject to complex solar and geomagnetic activity, making it very difficult to establish their functional relationship. To date, a strict physical ionospheric model has not been developed. In this section, characteristics of the ionosphere are studied first. Four existing ionospheric models are then reviewed, including the Klobuchar ionospheric model (KIM), the global ionospheric map (GIM), the regional ionospheric map (RIM), and the station-based ionospheric map (SIM).

2.4.1 Ionospheric Characteristics

The ionosphere is a dispersive medium, at the height of approximately 60 to 1000 km. In this atmosphere segment, molecules are partially ionized, caused by

solar ultraviolet and X-ray. Therefore, ionospheric delay is frequency dependent. The refractive index *n* of phase (p) and group (g) propagation can be represented respectively as (Kaplan & Hegarty, 2005):

$$\begin{cases} n_p = 1 + \frac{c_2}{f^2} + \frac{c_3}{f^2} + \frac{c_4}{f^2} + \cdots \\ n_g = 1 - \frac{c_2}{f^2} - \frac{c_3}{f^2} - \frac{c_4}{f^2} - \cdots \end{cases} \tag{2.31}$$

The coefficients c_2, c_3, c_4 are the functions of electron density n_e, and $c_2 = -40.3 \cdot n_e\ \mathrm{Hz}^2$. Since the first order of the ionospheric delay accounts for more than 99% of the total, higher order terms are negligible. Equation (2.31) is rewritten as:

$$\begin{cases} n_p = 1 - \frac{40.3 \cdot n_e}{f^2} \\ n_g = 1 + \frac{40.3 \cdot n_e}{f^2} \end{cases} \tag{2.32}$$

After integrating the refractive index along the signal path, the range difference caused by ionosphere refraction can be described as:

$$\begin{cases} \Delta S_p = -\frac{40.3}{f^2} \int_{user}^{satellite} n_e \, ds = -\frac{40.3TEC}{f^2} \\ \Delta S_g = \frac{40.3}{f^2} \int_{user}^{satellite} n_e \, ds = \frac{40.3TEC}{f^2} \end{cases} \tag{2.33}$$

while $\int_{\mathrm{user}}^{\mathrm{satellite}} n_e \, ds$ is the TEC per unit area along the signal path. Therefore, ionospheric delays can be obtained as long as TEC values are provided. Considering that the TEC values are usually given in a vertical direction (vTEC), an elevation angle-related mapping function is introduced to map them into LOS direction. As a whole, for one satellite-receiver pair and frequency f_i, the frequency-domain constraint is represented as:

$$\begin{cases} I_i = a_i \cdot F \cdot \frac{40.3\ vTEC}{{f_1}^2} \\ a_i = \frac{{f_1}^2}{{f_i}^2} \\ F(\varphi, h) = \left[1 - \left(\frac{R_e cos\varphi}{R_e + h}\right)^2\right]^{-\frac{1}{2}} \end{cases} \tag{2.34}$$

The mapping function $F(\varphi, h)$ is built on a thin-layer assumption proposed by JPL scholar — that the whole ionosphere section can be treated as a thin spherical shell at the height of 350—400 km typically (Lanyi & Roth, 1988) , as shown in Figure 2.6.

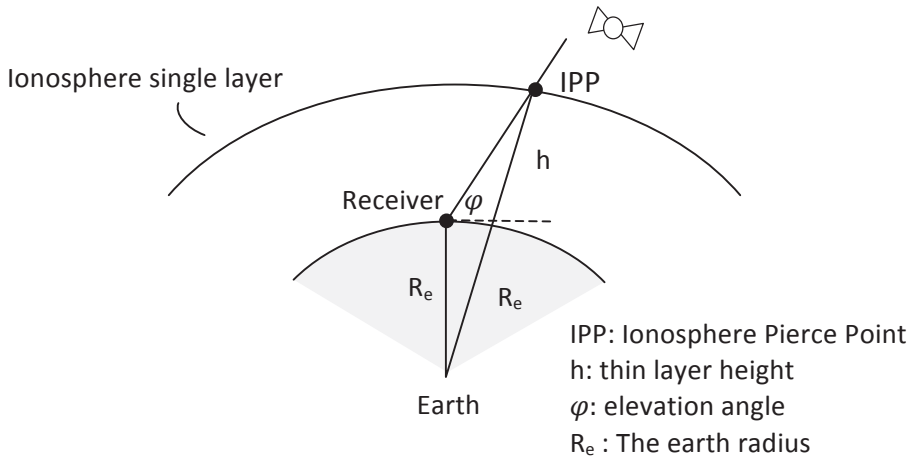

Figure 2.6 Ionosphere thin layer assumption

2.4.2 Existing Ionospheric Models

2.4.2.1 Klobuchar Ionospheric Model

Based on an empirical approach (Klobuchar, 1987), the Klobuchar model was designed to minimise the computational load and storage for single frequency users. This is a broadcast model, because coefficients are transmitted to users through satellites. Here is how the vertical delay is computed.

$$vTEC = DC + A \cdot \cos\left[\frac{2\pi(t - t_0)}{P}\right] \tag{2.35}$$

where DC is the night time delay as constant; A indicates the cosine function amplitude; t_0 denotes the corresponding local time of the cosine function peak; P stands for cosine function period; and t represents the local time of the ionosphere pierce point (IPP). A and P are derived from the following formulas:

(1) Calculate the earth-centred angle (elevation Ele in semicircles)

$$\psi = \frac{0.0137}{Ele + 0.11} - 0.022 \tag{2.36}$$

(2) Compute the latitude of the IPP (azimuth Azi in semicircles)

$$\emptyset_I = \emptyset_u + \psi \cos Azi$$

$$\emptyset_I = \begin{cases} +0.416, & \emptyset_I > +0.416 \\ -0.416, & \emptyset_I < -0.416 \end{cases} \quad (2.37)$$

(3) Compute the longitude of the IPP

$$\omega_I = \omega_u + \frac{\psi \ \sin Azi}{\cos \emptyset_I} \quad (2.38)$$

(4) Find the geomagnetic latitude of the IPP

$$\emptyset_m = \emptyset_I + 0.064\, \psi \cos(\omega_I - 1.617) \quad (2.39)$$

(5) Compute the amplitude and period of ionospheric delay

$$A = \sum_{n=0}^{3} \alpha_n \emptyset_m^n\,, \qquad P = \sum_{n=0}^{3} \beta_n \emptyset_m^n \quad (2.40)$$

where the eight coefficients α_n and β_n $(n = 1,2,3,4)$ are contained in the navigation message that describes only the main features of the ionospheric behaviour.

It is an empirical model, fitting from massive observations in global scale during the past decades. Due to its simplicity, only 50% of the ionosphere effect can be corrected (Klobuchar, 1987), achieving 4 m to 2 m positioning precision generally, which is far from enough for sub-metre level positioning.

2.4.2.2 Global Ionospheric Map

GIM, a public product provided by IGS, is defined in the ionosphere map exchange (IONEX) format (Schaer *et al.*, 1998). It is a 2.5°×5° grid map with a 2-hour temporal resolution, based on the thin layer assumption. Observation data from hundreds of IGS reference stations equipped with DF receivers around the world are collected to generate the GIM. The LOS TEC is derived from a geometry-free linear combination with a phase-smoothed code from the network. Then the slant value is mapped to the vertical direction, referred to as vTEC. The vTEC is then converted to a grid map employing spherical harmonic (SH) expansions with a full set of SH coefficients.

According to the IONEX format specification, users compute IPP latitude and longitude first, and then search for the nearest four grid points. An interpolation procedure is implemented to obtain vertical TEC values, which then are projected to slant ionosphere delays by a mapping function.

However, ionospheric characteristics cannot be described accurately at a large scale with one combined model. On one hand, the GIM accuracy is in the range of a 2 - 8 TEC Unit (TECU) ("IGS Data and Products," 2016), which cannot enable SF decimetre positioning. On the other hand, the IGS stations are primarily distributed in America and Europe. For countries like Australia and China, the reference station density is not sufficient for precise modelling. Additionally, the corrections are not available for real-time applications, due to the coarse temporal resolution and delayed update. IGS TEC map products are commonly used for post-processing applications and are available with a latency of less than 24 h or 11 days, respectively. The former is called rapid IGS ionospheric product and the latter is called final product.

2.4.2.3 Regional Ionospheric Map

RIM has a working mechanism that is similar to that at GIM, but is capable of providing more precise positioning results. That is because the regional inter-station distance (20-80 km) is shorter than the global reference station network. A denser ionospheric grid map can be generated, giving more details of the ionosphere. Temporal resolution of RIM is higher than that of GIM, as well.

SBAS systems take advantages of RIM data and broadcast signals through GEO satellites. There are a few other SBAS systems, such as the American WAAS, European EGNOS, Japanese MSAS. For regions without GEO satellite coverage, like Australia, a regional map can be transmitted through a terrestrial network. RIM is compared with GIM in several studies, with results illustrating the Root Mean Square (RMS) of ionosphere delay gets an improvement of 50 percent (H. Zhang et al., 2013).

2.4.2.4 Station-based Ionospheric Map

GIM and RIM introduce modelling errors when the ionosphere is assumed to be a single layer and a mapping function is used. A previous study demonstrated that this modelling error is about 0.05 to 0.2 m at different levels of ionospheric activities (Conte et al., 2011). In order to avoid this error, SIM utilises the slant ionosphere delay from a satellite to the reference station directly rather than the vertical TEC value from the grid map. A new study shows that the accuracy and precision of ionosphere delay predicted by SIM is 50 percent better than that predicted by RIM, with a baseline of 40 km (Li et al., 2014a). The proper use of auxiliary data, such as

DCB, will improve the result as well. Generally, utilising ionosphere delay predicted with SIM will reach a better result than with BIM, GIM, or RIM.

2.5 DISCUSSION OF POSITIONING DATA FORMAT STANDARDS

It is worth noting that the data exchange format is a crucial part of both RTK and PPP, since both techniques require large volumes of external information in real time. The information includes either raw observations or major error components. In accordance with how to provide the information in real time, and how to deal with major error sources, different standards are formulated. The radio technical commission for maritime services (RTCM) defines the internationally accepted data transmission standards for DGNSS, particularly by its Special Committee SC-104. RTCM version 3.0, whose transformation messages are demonstrated in Table 2.2, is the most popular format at the moment (Heo, Yan, Lim, & Rizos, 2009; RTCM, 2006).

With this RTCM3 standard, only the raw observations are provided. For each frequency of each signal path at each station, the lump sum of error components is represented in observation space, as demonstrated in Figure 2.7 (a). This method, called observation space representation (OSR), has been in operation in many services, primarily in RTK or network-RTK. But the problem is that the highly fluctuated ionospheric effect still affects the ambiguity-fixing problem for some receiver types (Wübbena, 2012).

To solve this problem, the state space representation (SSR) method was proposed by the RTCM-SSR working group. With this method, error sources can be represented as parameters of state vector and be estimated separately. It aims to provide major corrections in real-time, including common and individual error components for different signals, satellites and reference stations, as illustrated in Figure 2.7 (b). Compared to OSR, SSR is more promising. Firstly, it is unnecessary to observe different signals with SSR, as inter-signal biases are enough. Second, local station effects like multipath are greatly reduced. Thirdly, since only highly variable parameters are transmitted, SSR has a lower requirement on bandwidth than OSR.

Table 2.2 Basic message types for RTCM version 3.0

Group	Type	Content
GPS observations	1001	L1 only GPS RTK observables
	1002	L1 only GPS RTK observables including satellite signal-to-noise (CNR), full milliseconds for code observations
	1003	L1 and L2 GPS RTK observables
	1004	Extended L1 and L2 GPS RTK observables including satellite signal-to-noise (CNR), full milliseconds for code observations
Stationary antenna reference point	1005	Stationary RTK reference station ARP coordinates, ECEF XYZ
	1006	Stationary RTK reference station ARP coordinates with Antenna Height
Antenna description	1007	Antenna Descriptor
	1008	Antenna Descriptor and Antenna Serial Number

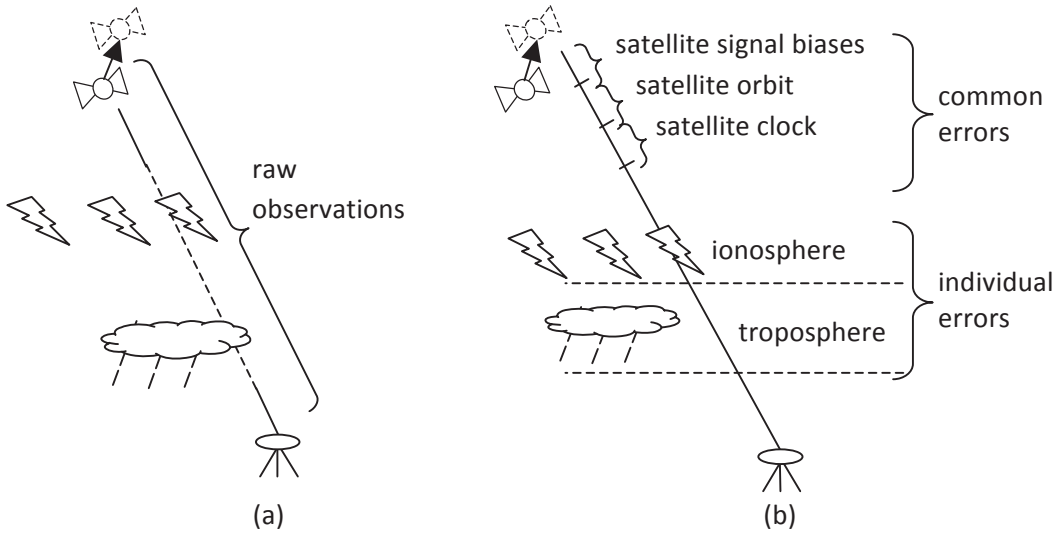

Figure 2.7 The methods for different standards. (a) Observation Space Representation; (b) State Space Representation

At present, the SSR concept is used only in these modes: post processing PPP, SBAS, and network-RTK that is partly derived from a state space model and converted to OSR (Wübbena, 2012). The major issue now is the standardisation of RTCM-SSR for real-time applications. The development plan for message exchange format includes three stages. In the first stage, the precise satellite orbits and clock,

and the code biases will enable the basic PPP mode: DF-RT-PPP. The second stage aims to enable SF-RT-PPP for most SF receivers by adding vTEC and satellite phase biases. Once the slant TEC is prepared, the PPP-RTK service will be enabled. Therefore, in the future, SSR can replace the OSR technique for all types of GNSS positioning applications, including RTK, with better performance and less cost.

The existing network-based processing modes are centralized. A general model was proposed by (Feng, Gu, Shi, & Rizos, 2013), that had station-based solutions generated at the station itself in a distributed manner. It is a unified model that PPP or RTK users can directly apply all the corrections from their nearby stations. These corrections may include receiver-specific parameters (clock, wet component of ZTD, instrumental code delay) and satellite-specific parameters (observable residuals, float ambiguity solution, tropospheric mapping function, ionospheric mapping function, vTEC and its standard deviation), plus elevation and azimuth angles. The data exchange format was defined as a site solution exchange (SITEX) format, making the station-based and user-based algorithms consistent with each other. In the research described herein, we primarily apply this station-based solution.

Chapter 3: Methods for GNSS decimetre positioning

This chapter describes the methods for GNSS decimetre level positioning, including generation of regional ionosphere corrections and user end positioning algorithms.

3.1 IONOSPHERIC CORRECTION GENERATION

3.1.1 Deterministic Representation with Stochastic Process

During Australian regional ionospheric correction generation, the slant TEC values along the signal paths for each station are computed from raw data to form the TEC products. These values are then converted to form the grid map RIM. Even though the overall concept is similar to the GIM provided by IGS, there is a fundamental difference in the extraction of the slant TEC values from the raw data.

Ionosphere delay varies in both time and space domains. Applying reasonable temporal-spatial constraints could increase the precision of its estimation (Shi et al., 2012). The common constraints include the spherical harmonic function (SHF) and polynomial model. For example, CODE has employed SHF, with an order of 15, to describe the global TEC distribution and its variation (Schaer *et al.*, 1998):

$$VTEC(\beta, s) = \sum_{n=0}^{n_{max}} \sum_{m=0}^{n} \tilde{P}_{nm}\,(sin\beta)\left(\tilde{C}_{nm}\,cos(m \cdot s) + \tilde{S}_{nm}\,sin(m \cdot s)\right) \qquad (3.1)$$

where β and s are the latitude and longitude respectively of the IPP; n is the order of the expansion; $\tilde{P}_{nm}$ denotes the Legendre function of m-power n-order; $\tilde{C}_{nm}$ and $\tilde{S}_{nm}$ are the unknown parameters.

Generally, the regional ionosphere is modelled using a polynomial model as follows:

$$VTEC(\beta, s) = \sum_{n=0}^{n_{max}} \sum_{m=0}^{m_{max}} E_{nm}\,(\beta - \beta_0)^n (s - s_0)^m \qquad (3.2)$$

where β_0 and s_0 are the latitude and longitude of the geometric centre of polynomial model; n and m are the orders of the model in terms of latitude and longitude; and E_{nm} represents the unknown ionospheric model coefficients.

The establishment of these two models usually involves employing data from tens or even hundreds of reference stations. The selection of the orders and degrees is dependent on the coverage of the station network and the observation timespan. Since in this research we require a model applicable not only to the regional grid map generation but also to the station-based ionospheric correction generation, we need a more general model to represent the ionospheric variation tendency over a single station. The following model is a second-order polynomial that describes the spatial characteristics,

$$VTEC(\beta, s) = a_0 + a_1 d\beta + a_2 d\beta^2 + a_3 ds + a_4 ds^2 \tag{3.3}$$

where a_0 denotes the average delay over the station; a_1, a_2, a_3 and a_4 are unknown coefficients of the polynomial model; $d\beta = \beta - \beta_0$ and $ds = s - s_0$ are the geomagnetic latitude and longitude differences between the IPP and the station.

One can introduce a stochastic process $r(t)$ to absorb the temporal biases that cannot be accurately described. It is dependent on its variogram:

$$2\gamma(t_i, t_j) = var(r(t_i) - r(t_j)) \tag{3.4}$$

If the following conditions are met, $r(t)$ is deduced as a second-order stationary process.

$$\begin{cases} E\big(r(t)\big) = \mu \\ cov\big(r(t_i), r(t_j)\big) = cov(t_i - t_j) \end{cases} \tag{3.5}$$

The mathematical expectation E of $r(t)$is constant, and the function $cov()$ is the covariogram. Under this assumption, the variogram can be simplified as:

$$2\gamma(t_i, t_j) = 2\big[cov(0) - cov(t_i - t_j)\big] \tag{3.6}$$

The spherical models can fit the experimentally derived variogram well:

$$\gamma(t_i - t_j) = \begin{cases} 0 & , t_i - t_j = 0; \\ c_0 + c_s \left\{ \frac{3}{2}\left(\frac{t_i - t_j}{a_s}\right) - \frac{1}{2}\left(\frac{t_i - t_j}{a_s}\right)^s \right\} & , 0 < t_i - t_j < a_s \\ c_0 + c_s & , t_i - t_j \geq a_s \end{cases} \tag{3.7}$$

where c_0 is the continuity of the stochastic process at the origin and a_s is the maximum time correlation span. c_s is the constant then the residuals become uncorrelated. Considering both systematic and stochastic features, a more accurate description can be obtained.

$$TEC(\beta, s) = F(\varphi, h)\left(a_0 + a_1 d\beta + a_2 d\beta^2 + a_3 ds + a_4 ds^2 + r(t)\right) \quad (3.8)$$

As noted previously, $F(\varphi, h)$ is the mapping function at the IPP.

3.1.2 The Reference Station-Based Computing Mode

Using the reference-station computing approach, the raw data streams from each GNSS reference station are processed individually, to generate the station-based corrections for the troposphere and ionosphere delays *dT* and *dI*, which can be used along with IGS precise orbits and clock products to support user-end positioning. The processing strategy is similar to the PPP technique excepting that the position vector of the station is held fixed (Gu, 2013). Accordingly, the observable residuals between observed values and computed values are derived as follows.

$$dP_i \equiv P_i - \left(\rho - c \cdot t^s + T_0 + I_{i0} - b^s_{pi-ref}\right) \quad (3.9)$$

$$= ct^r + tropm\, dZTD + \frac{f_1^2}{f_i^2} F(\varphi, h)(a_0 + a_1 d\beta + a_2 d\beta^2 + a_3 ds + a_4 ds^2 + r(t)) + b^r_{pi-ref} + e_{P_i}$$

$$dL_i \equiv L_i - \left(\rho - c \cdot t^s + \Delta\emptyset_{windup} + T_0 - I_{i0} - \lambda_{i0} N_{i0}\right) \quad (3.10)$$

$$= ct^r + tropm\, dZTD - \frac{f_1^2}{f_i^2} F(\varphi, h)(a_0 + a_1 d\beta + a_2 d\beta^2 + a_3 ds + a_4 ds^2 + r(t)) - \lambda_i dN_i + e_{L_i}$$

where $tropm$ is the tropospheric mapping function and $dZTD$ is the zenith troposphere delay (ZTD) correction, with respect to the empirical model T_0; N_{i0} is the approximate integer values of the ambiguity term Ni, while dN_i is the non-integer ambiguity components. The processing with (3.9) and (3.10) aims to determine all the biases in the right-hand side of Equation (3.9) and (3.10), including receiver-specific parameters (clock, residual ZTD, instrumental code delay), and the path-specific components (ionospheric parameters, and ambiguity term). The raw data on each frequency is used to aid estimation of ionospheric delays, which are then

estimated alongside other parameters such as phase ambiguities, ZTD, and receiver position and clocks. To minimize the convergence time, the I_{i0} may be computed from the GIM provided by CODE can be treated as *a priori* information of the slant ionospheric delay.

While all the biases in the Equation (3.9) and (3.10) are determined, plus the elevation and azimuth angles as part of outputs, they can be accessed by nearby users through the SITEX format, as shown in Feng *et al.* (2013), making the station-based and user-based algorithms consistent with each other. Since the ionospheric delays vary rapidly, quality control is especially required for reliability. Therefore, their standard deviations are provided as well. As a result, SIM is generated from the ionospheric corrections in the SITEX files, and RIM is then established for the IPP layer using the models given at the beginning of this section. In addition, this method particularly supports ambiguity-fixed PPP. Through SD between satellites, the receiver clock bias is cancelled, so the integer nature for carrier phase ambiguity resolution is preserved.

3.2 DATA PROCESSING STRATEGY AT A USER END

In the course of linearisation with SPP or the SF-PPP mode, the biases are either estimated or corrected, with respect to the standard SPP models, based on the broadcast messages for satellite orbits, clocks and ionosphere models. In this section, we focus on the biases that need corrections at the user end. According to Equation (2.3), their lumped bias can be expressed as:

$$dB_{Pi} = d\hat{\rho} - cdt^s + dT_0 + dI_{0i} - db^s_{obs-ref} \tag{3.11}$$

$$dB_{Li} = d\hat{\rho} - cdt^s + dT_0 - dI_{0i} + \Delta\emptyset + \lambda_i dN_i \tag{3.12}$$

where the subscript Pi means the i^{th} frequency of pseudorange; Li is the i^{th} frequency of the carrier phase. The remainder of this section is organised as follows. The ionospheric delay corrections are introduced in Section 3.2.1. The DCB correction is then discussed in Section 3.2.2. In Section 3.2.3, corrections for satellite attitude effects are analysed, among which the satellite antenna offsets are added to the satellite coordinate r^s, contributing to the range correction $d\hat{\rho}$; The phase wind up correction corresponds to the term $\Delta\emptyset$. Section 3.2.4 discusses the corrections

considered for the rover coordinate r_r, due to the solid earth tides and ocean loading. They are included in the range correction term $d\hat{\rho}$ as well.

3.2.1 Ionospheric Delay Correction

From a user's perspective, with RIM, one first finds the two nearest epochs i and $i + 1$ according to one's universal time t on the ionosphere layer. One then finds the nearest four points for one epoch to interpolates one's own ionosphere delay according to latitude λ, longitude φ, as illustrated by Figure 3.1. A simple four-point formula should be adequate:

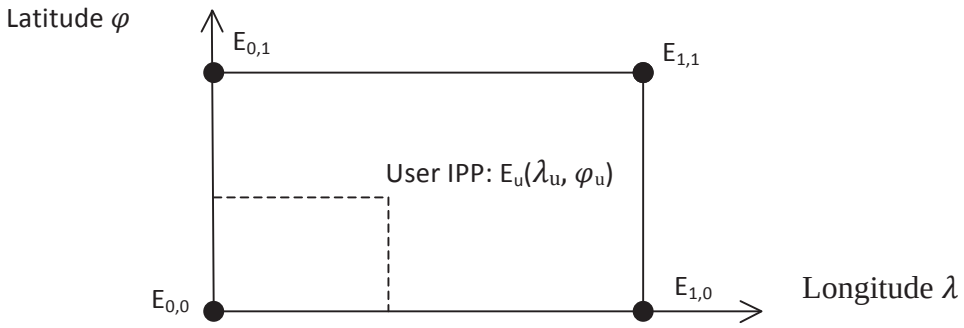

Figure 3.1 Ionospheric delay correcting strategy with RIM

$$E_u(\lambda_u, \varphi_u) = (1-p)(1-q)E_{0,0} + p(1-q)E_{1,0} + (1-p)qE_{0,1} + pqE_{1,1} \quad (3.13)$$

where $0 \leq p < 1$ and $0 \leq q < 1$. Repeat the same step for another nearest epoch, and do linear interpolation temporally between consecutive TEC maps:

$$E(\lambda, \varphi, t) = \frac{T_{i+1} - t}{T_{i+1} - T_i} E_i(\lambda, \varphi) + \frac{t - T_i}{T_{i+1} - T_i} E_{i+1}(\lambda, \varphi) \quad (3.14)$$

where $T_i \leq t < T_{i+1}$.

With SIM, users may access a nearby station and directly apply the same correction for that station. But it is only applicable for the short baseline and the high elevation angle, since ionosphere delay is location and elevation-dependent. The complete SIM method is to select several surrounding stations in the range of a certain baseline length threshold and to interpolate the correction of each LOS signal for user receiver ($sTEC_{user}$) with slant TEC values of surrounding stations ($sTEC^{ref}$), according to their relative geographical locations (D_{user}^{ref}):

$$sTEC_{user} = \frac{\sum_{ref=1}^{n} \frac{sTEC^{ref}}{D_{user}^{ref}}}{\sum_{ref=1}^{n} \frac{1}{D_{user}^{ref}}} for \quad (D < threshold) \tag{3.15}$$

Figure 3.2 demonstrates the concept. When employing SIM, the obvious advantage is that users do not need to receive very much data. Only the data from surrounding base stations is necessary. Therefore, SIM has the potential for real-time applications. Another advantage is that, by weighting it is possible to test and exclude some stations whose data is of bad quality, for further precision improvement.

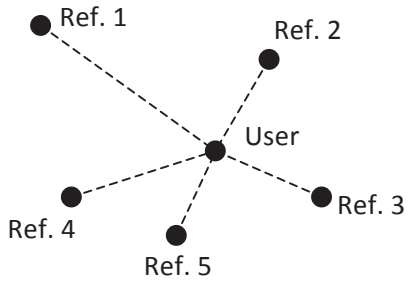

Figure 3.2 Ionospheric delay correcting strategy with SIM

3.2.2 DCB Correction

It is very difficult to synchronize the clocks in both satellite and receiver, because of differential code biases (DCB). These hardware instrumental biases - the time delay between observed and referenced pseudorange $\Delta t^{s}_{obs-ref}$ - introduce systematic errors when estimating ionosphere delays (Sardon, Rius, & Zarraoa, 1994),

$$I_{1,r}^{s} = \frac{P_{1,r}^{s} - P_{2,r}^{s}}{1-\gamma} - \left(\frac{b^{s} + b_{r}}{1-\gamma}\right) \cdot c + \frac{m_{2,r}^{s} - m_{1,r}^{s}}{1-\gamma} + \frac{v_{2,r}^{s} - v_{1,r}^{s}}{1-\delta} \tag{3.16}$$

where m and v stand for multipath and noise respectively. The time of group delay (T_{GD}) is the difference of the time from generation to transmission for L1 and L2 signals (L1-L2 correction). This can be obtained from the navigation message, and its clock is referenced to P1. For P2 measurement, Δt^{s}_{P2-P1} is directly related to T_{GD} by frequency (Rho *et al.*, 2007).

$$b^s_{P2-P1} = (\gamma - 1)T_{GD}, \qquad \gamma = \frac{{f_1}^2}{{f_2}^2} \tag{3.17}$$

Apart from DCB, the inaccurate satellite clock measurement could introduce decimetres of error, making combining pseudorange data with IGS precise clock products necessary. These products are referenced to C1. Therefore, T_{GD} and $b_{obs-ref}$ should be stamped on satellite clock errors, while ref depends on whether the precise clock correction is applied. For P1 measurement, b^s_{P1-P1} equals zero.

$$correction\ of\ t^s = \begin{cases} t^s - T_{GD} - b^s_{P1-P1} & without\ precise\ clock \\ t^s - T_{GD} - b^s_{P1-C1} & with\ precise\ clock \end{cases} \tag{3.18}$$

However, T_{GD} and DCB do not need to be taken into account for all kinds of users. Receivers working in relative positioning mode can eliminate the impact of DCB by the double differencing technique. DF receivers using ionosphere-free linear combination need DCB calibration but not T_{GD}. Only SF receivers working in absolute positioning mode require the external DCB calibration, which has been provided by CODE's monthly generated P1-CI table.

SF-PPP solutions at station BALA on 1 January 2014 are demonstrated in Figure 3.3. They are the daily east, north, up (ENU) differences between without and with CODE's monthly DCB correction. The IGS precise products are applied. Ionospheric delay is eliminated by SIM corrections that were generated with the method in Section 3.1. Tropospheric delay T_0 is computed with the Saastamoinen model. All other subordinate error sources, including satellite antenna offset, phase wind-up, and solid earth tides effect, are considered. The positioning performance gauged by RMS values with the unit in metres is indicated in the figure, with the all-corrected solution on the right and the DCB-uncorrected solution on the left. In this case, not applying DCB corrections can generate 0.2 m positioning error at maximum in East-West direction at 6 a.m. Figures 3.4, 3.5 and 3.6 use the same collection of data and are configured the same way.

3.2.3 Satellite Attitude Effects Correction

3.2.3.1 Satellite Antenna Offsets

Precise positioning has many more elements to be considered beyond DCB.

Correcting satellite-dependent errors concerns the discrepancy in force reference. The measurements are made to the antenna phase centre. So are the orbits broadcasted in navigation messages. However, the IGS-released precise satellite coordinates and clock products refer to the satellite centre of mass (Kouba *et al.*, 2001). Therefore, corrections on the phase centre offset (PCO) and even the phase centre variation (PCV) are compulsory if IGS precise ephemeris and clock are applied.

Figure 3.4 illustrates the daily 3-D difference between SF-PPP solutions without and with the PCO correction. The IGS08 model was applied. As shown in the figure, neglecting satellite antenna offsets can generate a 0.3 m positioning error at maximum in the east-west direction at 6:00 a.m.

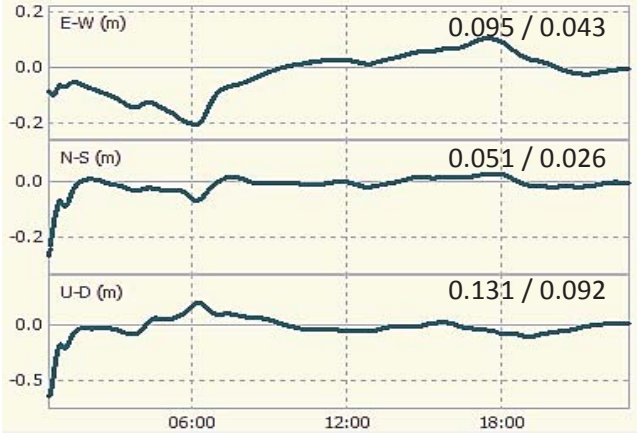

Figure 3.3 Difference between SF-PPP without/with DCB corrections

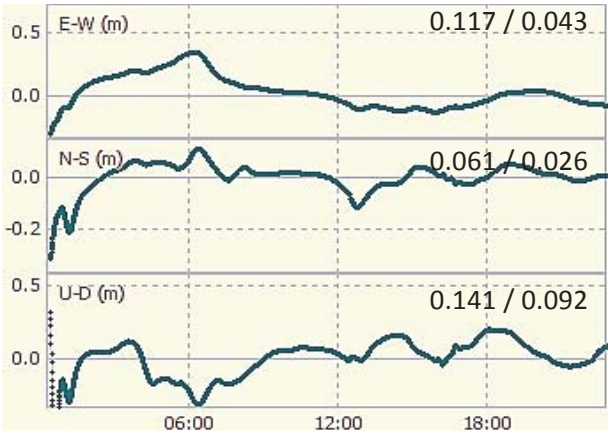

Figure 3.4 Difference between SF-PPP without/with satellite antenna offset corrections

3.2.3.2 Phase Wind-Up Correction

Phase wind-up effect needs to be taken into account when using carrier phase observations with undifferenced point positioning modes. Due to the right circular

polarization nature of the GNSS signal, a relative rotation of satellite and receiver antenna will cause a phase variation. That rotation usually results from the satellite keeping its solar panels pointing in the direction of the sun. For receiver antenna, this effect is fully absorbed into clock solutions or by differencing.

The correction can be computed according to (J. T. Wu, Wu, Hajj, Bertiger, & Lichten, 1993):

$$\delta\varphi = sign(\zeta) \cdot arccos\left(\frac{\overrightarrow{D'} \cdot \vec{D}}{\|\overrightarrow{D'}\| \cdot \|\vec{D}\|}\right) \tag{3.19}$$

where $\zeta = e \cdot \overrightarrow{D'} \times \vec{D}$, e is the unit vector from receiver to satellite, $\overrightarrow{D'}$ and $\vec{D}$ are two effective dipoles for the receiver (x, y, z) and the transmitter ENU coordinates (x', y', z'):

$$\overrightarrow{D'} = x' - e(e \cdot x') - e \times y'$$

$$\vec{D} = x - e(e \cdot x) + e \times y \tag{3.20}$$

Adding full cycle terms of $\pm 2\pi$ to the correction ensures continuity between consecutive phase observations.

Figure 3.5 shows the ENU difference between applying wind-up correction and not. The maximum error in the east-west direction reaches 0.1 m.

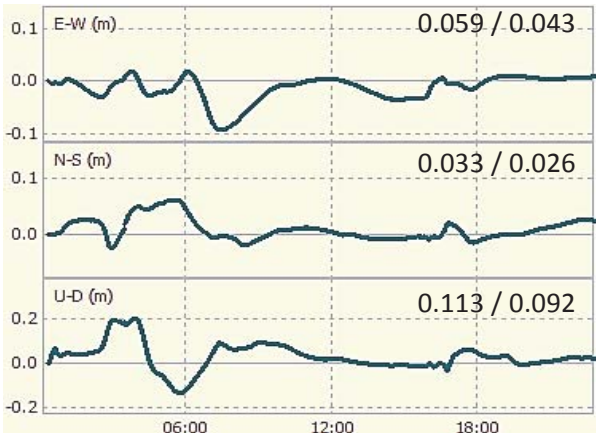

Figure 3.5 Difference between SF-PPP without/with phase wind-up corrections

3.2.4 Site Displacement Effects Correction

3.2.4.1 Solid Earth Tides

When decimetre or higher precision is required, the effect of solid earth tides should be taken into consideration. Because the stations are on the ground, there are

weakly fluctuated vertical and horizontal site displacements due to gravitational attracting forces from the sun and the moon. The magnitude of the effect depends on station latitude and tidal frequency (Wahr, 1981). A simplified model for the tide displacement can be found in (McCarthy, Dennis, & Petit, 2004). Omitting the solid earth tides effect, horizontal positioning precision could be degraded for 0.1 m at maximum, according to Figure 3.6.

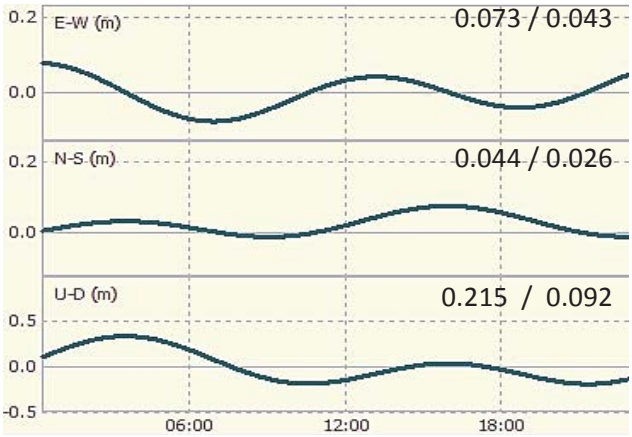

Figure 3.6 Difference between SF-PPP without/with solid earth tide corrections

3.2.4.2 Ocean Loading

Ocean loading is a second order effect that results from the load of the ocean tides. It is more localized, and can be neglected with centimetre accuracy PPP mode for stations that are far from the oceans.

3.3 COORDINATE SPACE REPRESENTATION

RTCM standards have been widely used for transmitting information to users in precise positioning modes such as network and single-based RTK. Regardless of network or single baseline computing modes RTCM messages combines the reference station GNSS raw data with error corrections. The RTCM corrections are provided in a “lump sum” as in observation space representation (OSR). For PPP positioning and precise SPP, the more prospective standard RTCM –SSR will be applicable. The SSR is designed to transmit error correction messages in components separately in the state space. This means that these services are only applicable for GNSS devices that can output measurements. However, many types of low-end GNSS devices, such as GNSS units in mobile phones, do not output raw measurements. It is difficult for these devices to improve the SPP accuracy.

We now propose coordinate space representation (CSR) messages for RTCM-OSR or RTCM-SSR formats to support improvement of low-end GNSS device positioning accuracy. The CSR messages include five terms for each satellite: 3 LOS terms, 1 lumped correction term and 1 sigma term for the lumped correction for a real or virtual reference station. On receiving the CSR information, an user receiver is able to correct its own coordinates with the time tags and PRNs that have been used in computation of it SPP coarse position coordinates. Alternatively, if the server end receives the time tags, the PRN information and the coarse SPP solutions from users, their SPP solutions can also be corrected. In this process, raw measurements are neither required from server end nor at user end.

We now theoretically prove why the coordinate bias $\boldsymbol{dX}(\Delta x, \Delta y, \Delta z)$ can be corrected by the five term CSR messages of a reference site nearby. From (2.6), at a reference station, we have the linear equation:

$$\boldsymbol{dP - dB = HdX + e} \tag{3.21}$$

where $\boldsymbol{dB}$ can be expressed/computed by (3.11). The least square solution of (3.21) can be obtained by

$$\boldsymbol{d\widehat{X} = (H^T H)^{-1} H^T (dP - dB) = (H^T H)^{-1} H^T dP - (H^T H)^{-1} H^T dB} \tag{3.22}$$

At a rover nearby,

$$\boldsymbol{dP_1 - dB_1 = H_1 dX_1 + e_1} \tag{3.23}$$

The least square solution can also be expressed by

$$\boldsymbol{d\widehat{X}_1 = \left(H_1{}^T H_1\right)^{-1} H_1{}^T (dP_1 - dB_1)}$$

$$\boldsymbol{= \left(H_1{}^T H_1\right)^{-1} H_1{}^T dP_1 - \left(H_1{}^T H_1\right)^{-1} H_1{}^T dB_1} \tag{3.24}$$

If the same set of satellites are used at the base and rover receivers, then

$$\boldsymbol{dB_1 \approx dB, \quad H_1 \approx H} \tag{3.25}$$

$$\boldsymbol{d\widehat{X}_1 = \left(H_1{}^T H_1\right)^{-1} H_1{}^T dP_1 - (H^T H)^{-1} H^T dB} \tag{3.26}$$

The second term is the same as the second term for the base station. Therefore, in theory the coordinate bias at one station can improve the coordinate for its surrounding rovers. Users do not have to output raw observations in order to obtain the improvement, but output the PRN information.

To be precise, CSR messages should be part of RTCM-OSR or RTCM-SSR standards to serve more devices. CSR messages are much simpler and the message size is very small. The required additional bandwidth is very low. From users' perspective, the additional computation $(\boldsymbol{H^T H})^{-1}\boldsymbol{H^T dB}$ can be easily completed at low-end terminal such as mobile phones. The computations can also be done for the rovers at the server end.

It should be noted that there are some limitations in CSR-based improvement. First, the accuracy of the SPP solutions depends on the accuracy of the ionospheric delay or inter-station distances of the network. Secondly users' internal SPP algorithms should be consistent to the algorithms $(\boldsymbol{H'H})^{-1}\boldsymbol{H^T dB}$, in order to maximize the accuracy improvement. Time tag, PRN, and coarse coordinates must be available to the server. This problem can be solved by duplex communication since smart phone applications know the satellites they are using. It is understood that both android and iOS systems provide this data, however, the author has not inspected the iOS source code.

Chapter 4: Results

4.1 ARRANGEMENT OF EXPERIMENTS

Experiments in this study are designed to evaluate the ionospheric correction generation methodology explained in Section 3.1, to test the user-end processing strategy discussed in Section 3.2, and finally to demonstrate that ionosphere delay corrections can support decimetre positioning. Three sets of experiments are conducted:

1) Australian ionospheric maps generation and their evaluation with high-end CORS receivers in static mode;
2) Australian ionospheric maps evaluation with low cost U-blox receiver in dynamic mode;
3) CSR representation using Australian ionospheric corrections.

The test results are discussed in terms of: ionospheric map quality; interpolated SIM performance; static positioning performance with high-end receivers; dynamic positioning with low-cost receiver; and the usage of the ionospheric map on the CSR solution. Analyses elaborate how ionosphere delay corrections from around 200 stations in Australia can support SF SPP and PPP for decimetre solutions.

High quality pseudorange and phase measurements were collected on 1 January 2014 from about 200 stations within Australia for RIM and SIM generation, as represented with red dots in Figure 4.1. The 25 stations treated as user receivers are marked in blue dots. CODE-released GIM is used for comparison. It is generated from 400 global stations, but only 20 of which are mounted in Australia, as illustrated in green.

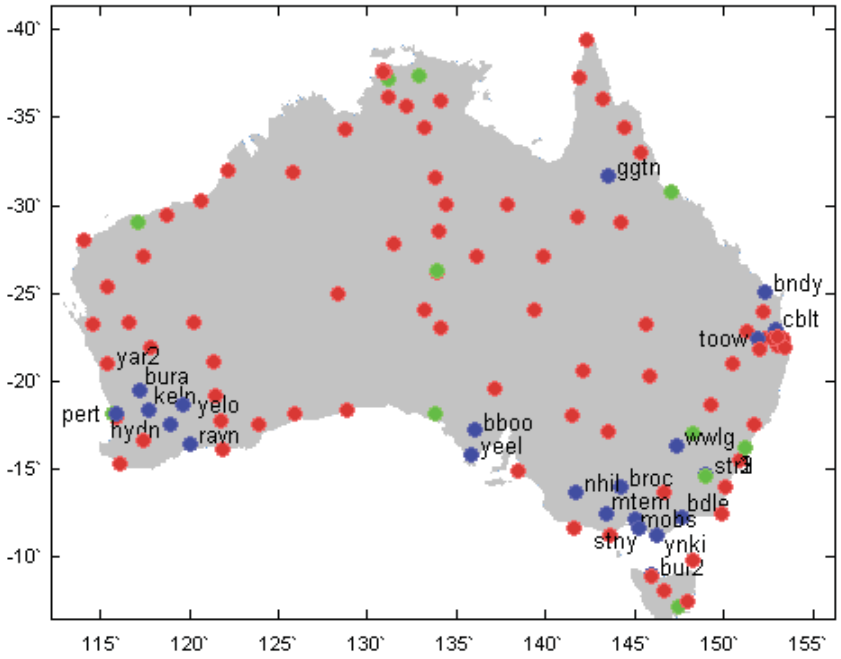

Figure 4.1 Australian stations employed for ionospheric correction generation

4.2 QUALITY EVALUATION OF AUSTRALIAN IONOSPHERIC CORRECTIONS

Figure 4.2 demonstrates the spatial resolution of these two ionospheric grid maps covering -55° - 0° (latitude) and 105° - 165° (longitude). Evidently, Australian RIM (bottom row of figure) provides more detailed ionosphere characteristics because of the higher station density and its appropriate algorithm. To evaluate the RIM and GIM quality, the LOS TEC values in the station-based map are regarded as the true value. The differences between global or regional vTEC and the "real" vTEC are presented with an increasing elevation angle in Figure 4.3. Each calculation is conducted at the same IPP latitude and longitude. Specifically, the station-based map is updated every epoch (30 seconds) and the regional map is updated every five minutes. Since the vertical ionosphere delay is fairly stable within 10 minutes (Blanch, 2003), the five-minute resolution is short enough to provide high accuracy in this experiment. The spatial resolution for both global and regional map is 2°×2.5°. There is a descending trend in the difference with the elevation growing, because the lower elevation introduces a greater mapping error when converting the ionosphere delay from slant to vertical, and vice versa. The 1σ RMS values are 3.2 TECU for GIM, and 0.6 TECU for RIM.

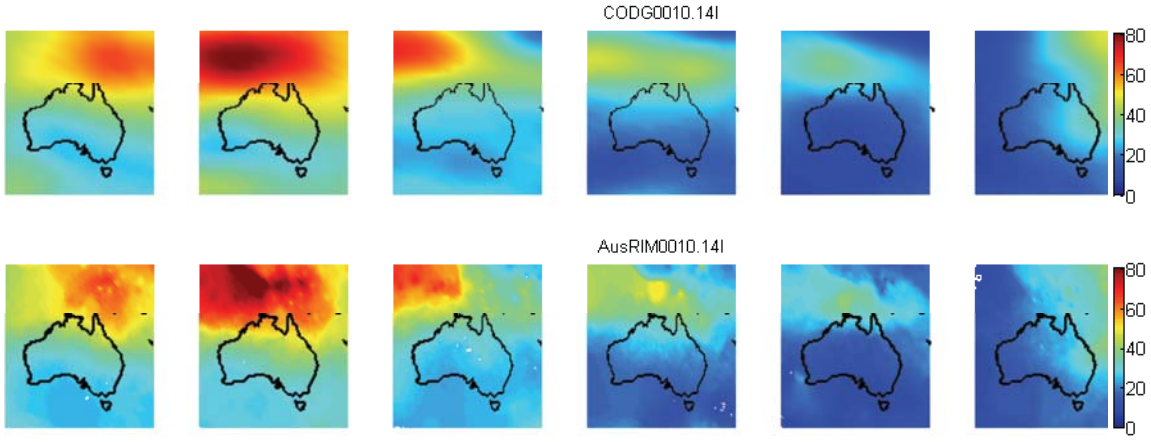

Figure 4.2 Australian vTEC maps provided by GIM (top row) and RIM (bottom row) at epochs 0200UT, 0600UT, 1000UT, 1400UT, 1800UT, 2200UT from left to right columns

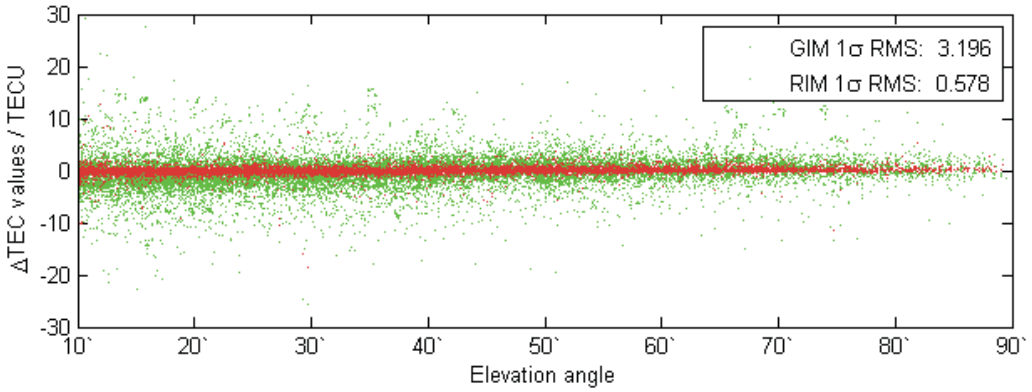

Figure 4.3 Quality analysis of GIM and RIM, represented by the differences between grid map vTEC and station-based vTEC

4.3 SIM PERFORMANCE

When applying the reference station-based processing approach introduced in Section 2.1, positioning results using SIM corrections with different baseline lengths are calculated at the 25 user receivers (plotted in Figure 4.1 as blue dots). The baseline length threshold as radius is selected from 150 km to 300 km, with a step of 50 km. The longer radius leads to more surrounding stations being included. The SPP and PPP results at three directions, demonstrated separately in Figure 4.4 and 4.5, show that it cannot be concluded that the positioning precision is positively or negatively correlated with the increase of surrounding station numbers. For example, station BURA, whose surrounding stations are symmetrically distributed according to figure 3, shows that the more stations included, the better the precision is obtained on both modes and in all directions; however, for station BNDY, with all the surrounding stations on its south side, the more stations utilised, the more southern they are to the user, which leads to precision degradation. Similarly, all the baseline

distances for GGTN within 300 km are around 280 km, rendering the distance-dependent ionosphere correction inaccurate. In this case, the station geometrical distribution needs to be quite symmetrical and compact. Under most situations, a radius of 300 km is appropriate in order to cover five surrounding stations on average. Users in locations like BNDY should take the correction from the nearest station instead of by interpolation.

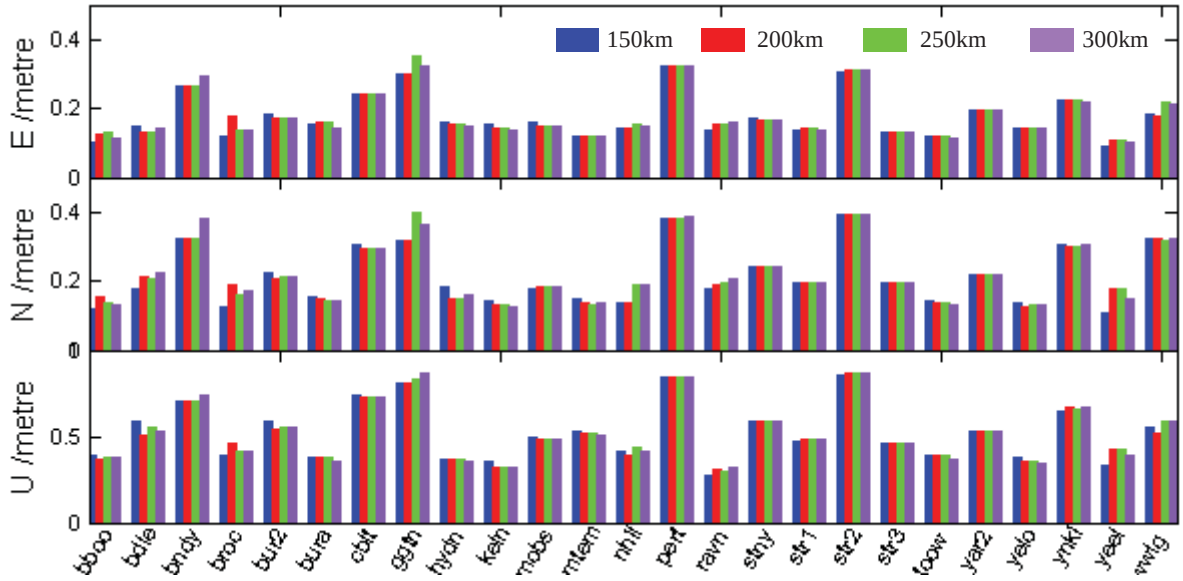

Figure 4.4 SPP positioning precision: SIM with different radius lengths

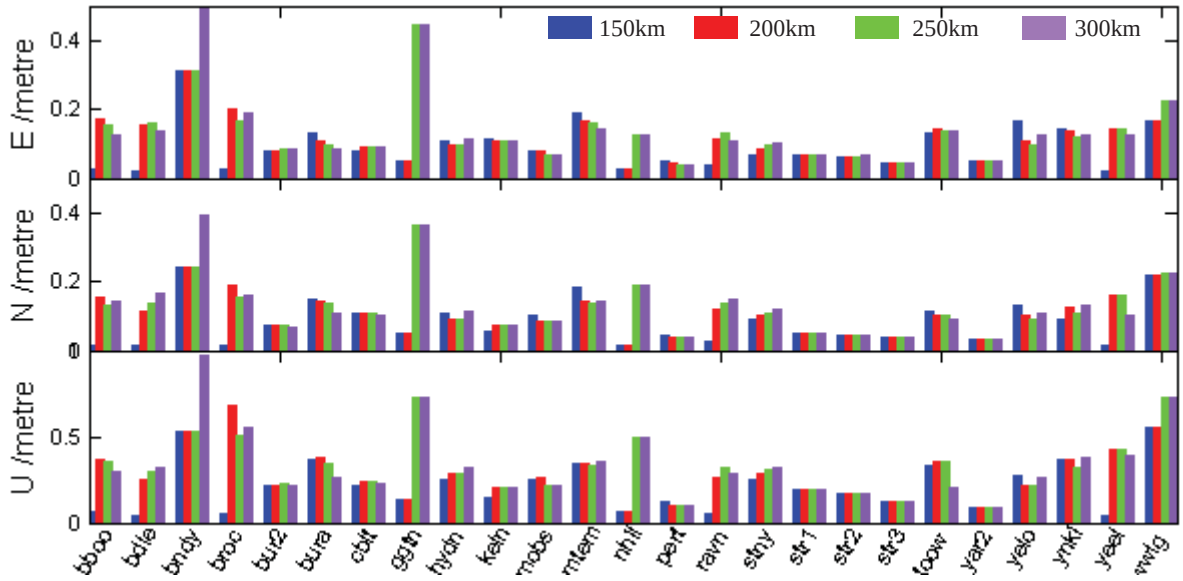

Figure 4.5 PPP positioning precision: SIM with different radius lengths

The quality of the ground-interpolated SIM method is further analysed through combining the biases for all satellites above the cut-off angle of 10°. Figure 4.6 (upper panel) gives an example at station STR2, where there are several outliers:

biases of PRN 24 and PRN 4 (the inserted part) reach -4 and -6 TECU, which will cause large errors of 0.64 m and 0.96 m respectively along their L1 signal paths. These obvious deviations can be easily eliminated. Then the RMS values of biases are calculated and plotted (lower panel in Figure 4.6) epoch to epoch. The RMS through the whole day is then calculated, and equals 0.226 TECU, which corresponds to a few centimetres, indicating that as a whole the error of interpolating with surrounding stations is acceptable for decimetre level applications. Figure 4.7 shows the all-day RMS for the 25 user receivers in total, 68% of which are under 0.5 TECU.

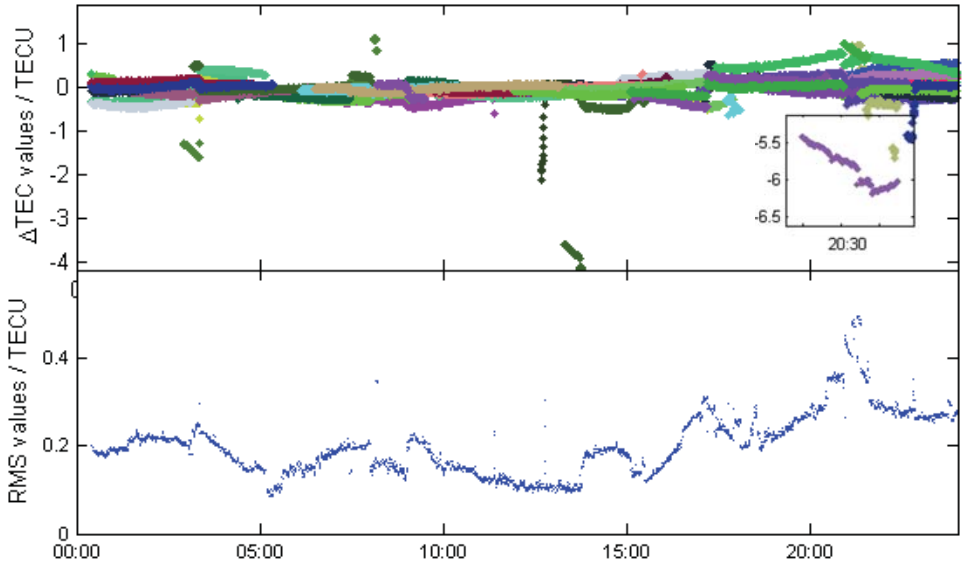

Figure 4.6 Biases for all satellites through the whole day and the RMS values of biases

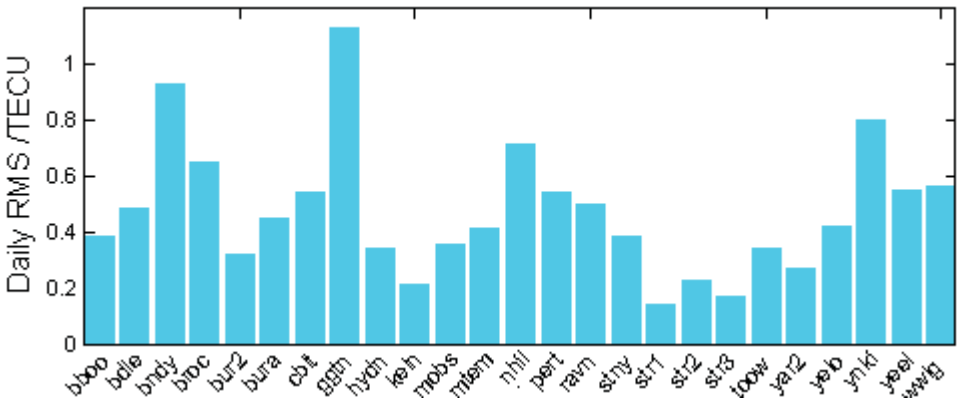

Figure 4.7 RMS values for 25 user receivers

4.4 POSITIONING RESULTS

4.4.1 Static Positioning

With this analysed station-interpolated SIM method, the five-minute updated RIM, and the CODE-GIM ionospheric corrections, the all-day SPP and SF-PPP positioning results at station TOOW are plotted (see Figure 4.8). Good consistency is evident between SIM and RIM solutions, while the GIM deviations have greater fluctuations, especially in the vertical direction. Figures 4.9 and 4.10 separately show the ENU RMS values of all 25 user receivers on the two modes. It is interesting to note that solutions using the RIM sometimes give an even better epoch-to-epoch accuracy than using the SIM approach. More specifically, their 1σ RMS values are summarized in Table 4.1. The SPP solutions from 25 selected reference receivers prove the decimetre RMS values using Australian regional ionospheric corrections, which is reduced from 32 cm to 19 cm for the east/north component and from 72 cm to 55 cm for the up component, compared to the GIM method. With the same data sets and receivers, the SF-PPP mode reduces the RMS values from 25 and 55 cm to 13 cm and 34 cm in the two components. It can be seen that SIM improves the performance of the SF-PPP solution by approximately 15 cm in two directions.

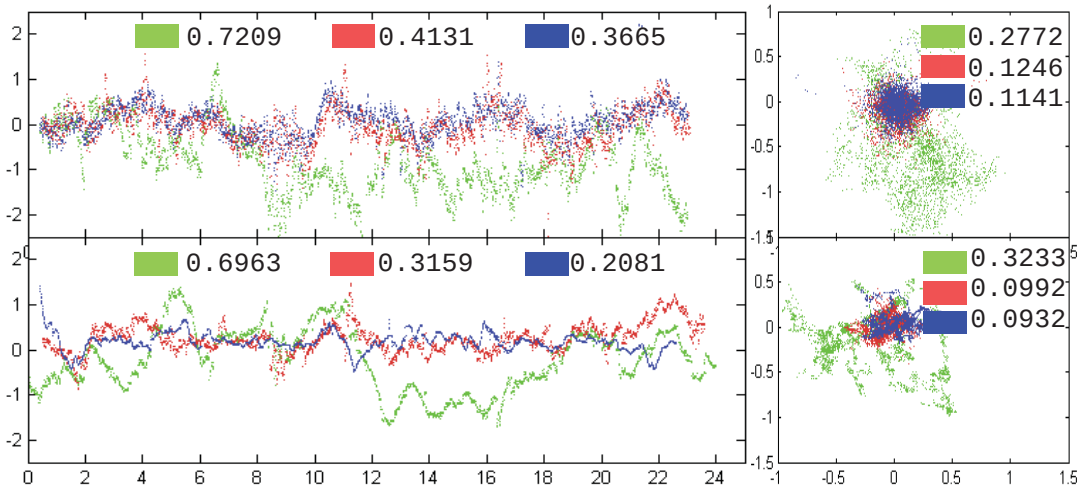

Figure 4.8 Positioning deviations at station TOOW on both SPP (top row) and PPP (bottom row) modes, with three different ionosphere corrections (GIM in green, RIM in red, and SIM in blue). Results are represented in vertical (left column) and horizontal (right column) directions

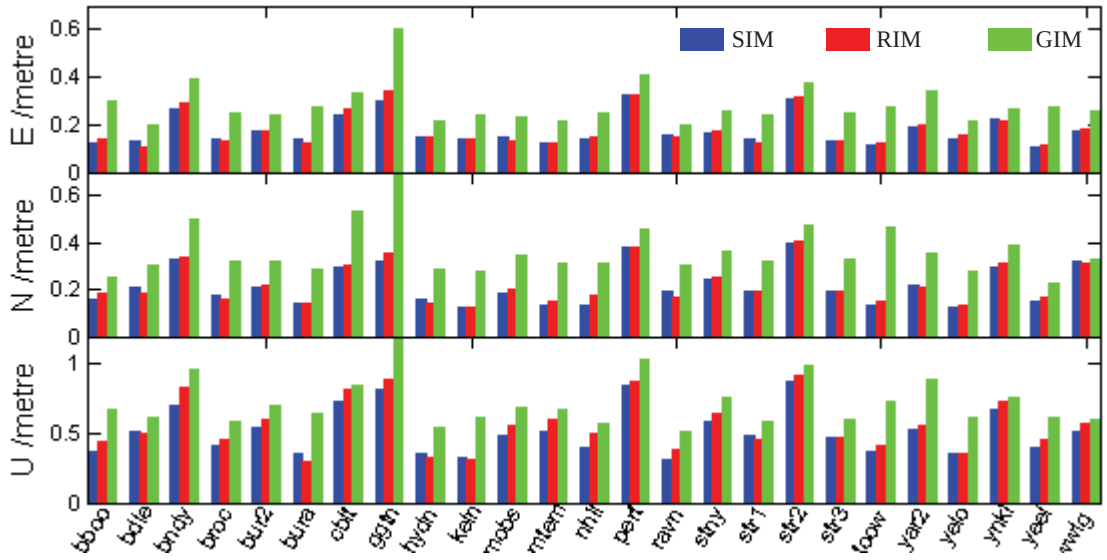

Figure 4.9 Positioning precision at East, North, Up directions for 25 stations on SPP processing mode with GIM, RIM, and SIM corrections respectively

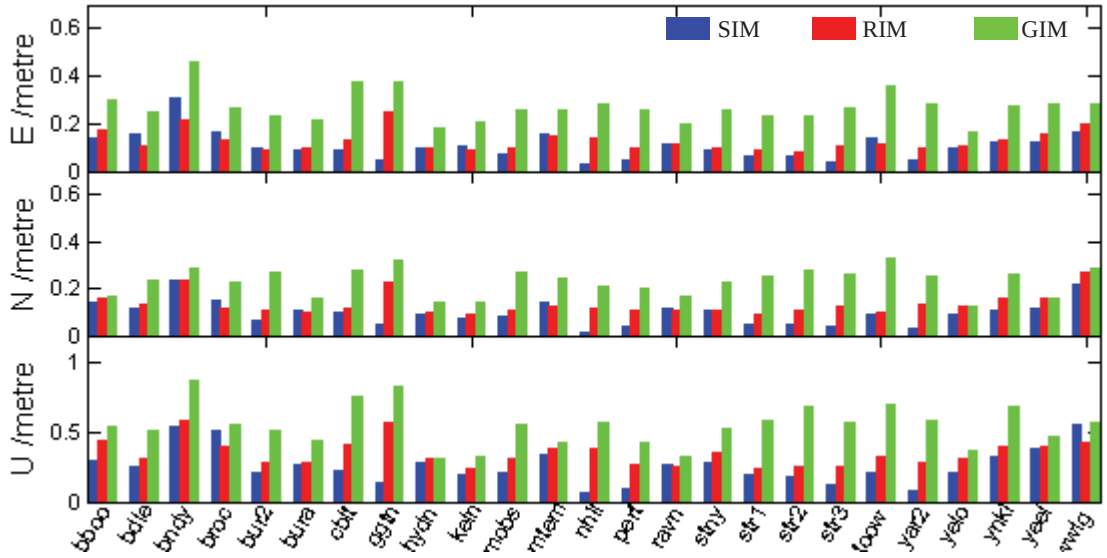

Figure 4.10 Positioning precision at ENU directions for 25 stations on PPP processing mode, with GIM, RIM, and SIM corrections respectively

Table 4.1 Total RMS values in meters at three directions, computed with three ionospheric correction strategies on SPP and SF-PPP modes

RMS / m		SPP	SF-PPP
GIM	E	0.284	0.269
	N	0.360	0.227
	U	0.715	0.545
RIM	E	0.178	0.125
	N	0.222	0.131
	U	0.553	0.344
SIM	E	0.175	0.106
	N	0.216	0.096
	U	0.513	0.254

4.4.2 Dynamic Positioning with Low-Cost Receivers

A dynamic road scenario experiment was conducted on the 7 May 2016 along main roads in a Brisbane suburb. The route appears as an oblong shape, 1.5 km long (north-south) and 2.5 km long (east-west) approximately, as shown in Figure 4.11. Two sets of equipment are mounted on the roof of a vehicle:

1) Advanced configuration: NovAtel receiver with Trimble antenna;
2) Low-cost configuration: U-blox receiver with U-blox antenna.

Figure 4.11 Route of the road scenario experiment

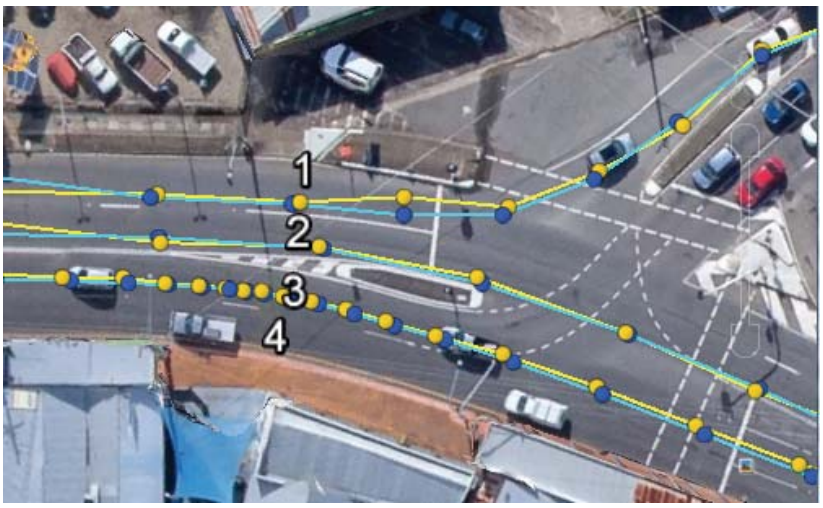

Figure 4.12 Four lanes of the roads, three of which was tested

At the user end, the five-minute updated Australian SIM was applied as the ionospheric effect correction model. Two sets of GNSS raw data are processed with the SF-PPP mode using the strategy discussed in Section 3.2. Figure 4.12 gives a clear snapshot of the road segment denoted in the red rectangle in Figure 4.11. The

direction is adjusted for better demonstration. It is a double-direction road, with two lanes in each direction. The numbers of the four lanes are marked in white. We drove back and forth twice. The two forward journeys were all in lane No.3, the return journeys were in No.1 and No.2. The positioning results with advanced and low-cost receivers are indicated by the blue and yellow lines, respectively. It is shown that both advanced and low-cost receivers can detect individual lanes. It can be seen that the yellow dots do not deviate far from the blue ones. This result demonstrates that our Australian slant ionospheric correction products works properly. It indicates that even low-cost receiver users such as car drivers are able to achieve sub-metre or even decimetre positioning precision (for example, lane detection) as long as SIM is accessed. It is noted that for every sample, the yellow position is half a metre ahead of the blue coordinate. That is because we intentionally set a half metre space for two antennas, to avoid interference.

4.5 COORDINATE SPACE REPRESENTATION

To verify the CSR method discussed in Section 3.3, a regional reference station network in south-western Australia was picked for the uniform distribution of its seven stations, as shown in Figure 4.13. They are KALG, YELO, NORS, BALA, HYDN, RAVN, and ESPA, in the order from lower to higher latitude. The set of raw data described in Section 4.1 was then processed with two strategies: the SPP mode with broadcast ionospheric correction (SPP_BRDC) and the SPP mode with SIM slant TEC ionospheric correction (SPP_TEC). The former is used to simulate mobile phone configurations but with lower noisy raw data. The latter reflects the term ΔB in Equation (3.19). Since the ionospheric effect dominates in SPP positioning precision, the only difference between the two strategies in this experiment is the ionospheric correction method. Therefore, the ENU positioning result biases of a station with two configurations should directly indicate the ionospheric delay over that station.

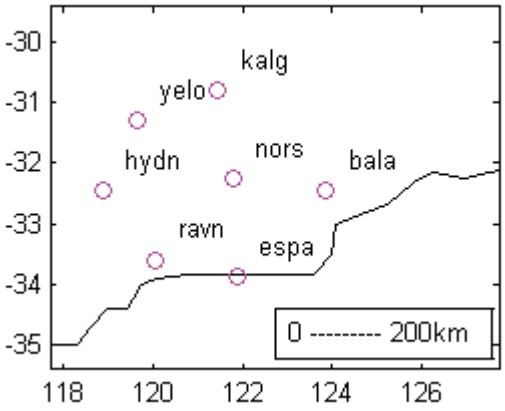

Figure 4.13 Distribution of the seven reference stations for CSR

We output the coordinate corrections, the biases of the two modes, for the seven adjacent stations in Figure 4.14. Generally, the results show great consistency, as the results at seven stations share the same pattern of fluctuation. That is because the temporal-spatial characteristics of the ionosphere over a local scale do not vary dramatically. A necessary condition for CSR strategy to be effective is that the satellites have to be consistently visible at two stations. Therefore, we eliminate the results of around two hours from 17:30 to 19:20. This part shows obvious outliers, because the visible satellites at each station vary a lot during this time. The overall consistency illustrates the validity of using coordinate bias at one station to improve the coordinate for its surrounding rovers.

To demonstrate the impact of distance on the coordinate precision, the station KALG is chosen as the reference station, and the rest six stations are treated as rover stations. Table 4.2 summarise the mean biases and standard deviation (STD) values relative to the reference station. For the data samples that have the same satellites at the rover stations, we apply the CSR corrections from KALG. From the nearest to the furthest station, the distances between rover and station range from 160 km to 350 km. The third column denotes the total data samples that use the same visible satellites as the reference stations. It indicates that the values of mean biases generally depend on the distances. The coordinate ENU discrepancies are seen to be less than 0.3 metres for the stations BALA, NORS, and YELO. Their distances to the reference station are within 300 km. It is also observed that there is a data gap of about two hours at RAVN. Similarly the ENU standard deviations of three directions become worse with the increase of distance to the reference station. Comparing with several to tens of metres errors in the normal SPP solutions with broadcast messages,

the CSR method has the capability to improve their positioning performance to a certain degree.

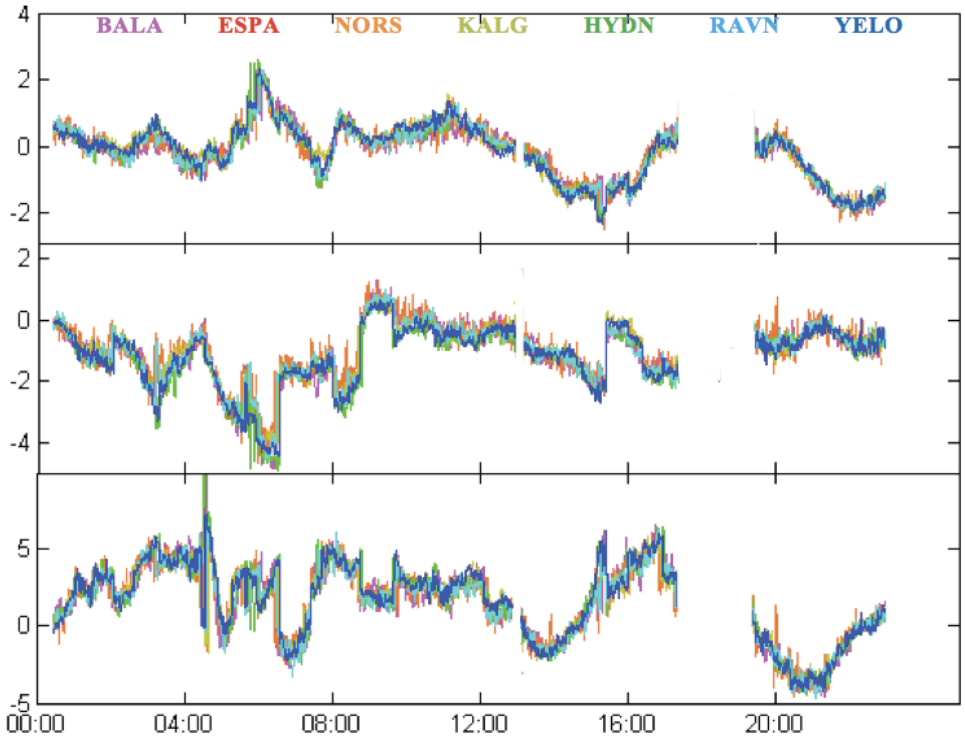

Figure 4.14 Coordinate biases of the two modes, for the seven adjacent stations

Table 4.2 The relationship between distance and the correcting precision

Station	Distance / km	Raw data numbers	Mean E	Std E	Mean N	Std N	Mean U	Std U
NORS	167	2683	0.004	0.142	0.168	0.323	0.107	0.727
YELO	181	2691	0.035	0.255	0.003	0.294	0.088	0.824
BALA	295	2673	0.030	0.220	0.164	0.372	0.094	0.781
HYDN	305	2660	0.002	0.279	0.121	0.368	0.155	1.042
RAVN	339	2178	0.061	0.295	0.212	0.474	0.303	1.196
ESPA	346	2610	0.009	0.167	0.280	0.433	0.091	1.018

Chapter 5: Conclusion

This chapter firstly outlines the work of this thesis and the significance of this study. Next the major contributions and outcomes are highlighted. Finally, this chapter discusses the potential future work.

5.1 SIGNIFICANCE AND SUMMARY

5.1.1 Significance

Single-frequency (SF) GPS receivers have the potential to become an accurate alternative to high-end dual frequency receivers for many applications such as GIS data collections, vehicle positioning for lane-level safety and traffic management applications For a single frequency receiver to achieve positioning precision of decimetre level, ionosphere delay is the main bottleneck among all error sources.

Research efforts were directed in the network end, user end, and experimental aspects. From the perspective of the server end, the vertical and slant ionospheric corrections were generated and their generation methods studied in depth. At the user end, importance was attached to how to take advantage of the ready-to-use ionosphere corrections. The objective of the experiments was to validate the developed approaches.

5.1.2 Summary

This thesis summarised various computation modes and multiple standards, and studied ionospheric models in the GNSS positioning area.

Section 2 summarised the basic equation for determination of platform position, velocity and time, and described the SPP mode. DGNSS is investigated subsequently, which eliminates the common error sources for both receivers by differencing. DGNSS is able to achieve extremely accurate positioning, though masses of resources consumption and hardware equipment are inevitable. SBAS provides corrections through satellite data link. It is designed to offer 1 to 2 m accuracy for SF users. These three modes are code-based. When using the carrier-phase measurements, RTK and PPP modes give precise positioning performance. By DD, RTK enables centimetre precision with very short observation time. Besides,

DF-PPP and PPP-AR techniques is analysed in this thesis. All of them are presented thoroughly in terms of maths, of handling biases and errors, and of pros and cons.

Not only modes but also various standards of data link are summarized including RTCM and RTCM-SSR standard. In conclusion, the SSR strategy is prospective, with the major issue of its standardisation. Furthermore, this thesis proposed a CSR format, to support low-end GNSS devices from which the raw data is not accessible. Theoretical analysis and experimental results demonstrated its potential to improve the positioning precision. But the time tag, PRN, and coarse coordinates must be available to the server.

For dealing with error sources, the major challenge, namely, ionospheric effects, is investigated. Practical models are developed given known Ionospheric characteristic. Conventional KIM and the more accurate (and prevalent) GIM are reviewed. The attention is focussed is on RIM and SIM. It is explained how utilising SIM ionosphere delay predictions yields better performance than KIM, GIM, and RIM.

5.2 MAJOR CONTRIBUTIONS AND OUTCOMES

This thesis contributes the following.

- A systematic analysis of existing error correction techniques is detailed.
- An improved (CSR) method is developed.
- Real-world experiments and data processing are carried out to verify the new method.

By conducting experiments thoroughly and analysing the results, this thesis has strengthened knowledge about less-developed regional ionospheric correction in Australia, and has validated the benefits of regional ionospheric corrections on SF GNSS receivers for achieving decimetre positioning.

5.2.1 Ionospheric Correction Generation

In the extraction of the slant TEC values from raw data, this thesis synthesized deterministic representation with stochastic process applicable for a single station, based on the correlation of its temporal-spatial distribution. Australian SIM and RIM are derived from hundreds of stations nationwide. This thesis conducted a

comparison of the GIM and RIM models. With a denser network and a higher processing rate, the quality of the regional map gauged by its RMS value is proved to range from 0.2 to 1 TECU referred to SIM, which is much smaller than the 3.2 TECU RMS of the global map. This had been intuitively spotted from 3-D maps of the two VTEC maps. Their accuracy difference was further reflected in the ENU positioning results.

5.2.2 Data Processing Strategy at the User End

In this research, the user end strategy is developed by considering all the elements that could affect GNSS decimetre positioning. These effects are expressed mathematically and quantitatively. With the PPP-like unified model, the measurements from each GNSS reference station are processed individually, to generate station-based solutions. For users, this model avoids having to employ data from a regional or global network consisting of hundreds of reference stations.

How to take advantage of the generated ionospheric maps was of major concern. The SIM interpolation method is explained in detail. Instead of accessing a nearby station and directly applying the exact correction for that station, it is more pragmatic for a user to interpolate a correction according to its nearby stations. Based on a new module development on RTKLIB software platform, this paper, which especially evaluated the station-based interpolation approach with SIM by calculating the epoch-to-epoch and all-day RMS errors of each signal path, concludes that quality of interpolating with surrounding stations is acceptable for sub-meter or decimetre level applications. In addition, by this method, data of bad quality was excluded easily. From the experimental results, it is concluded that a baseline length of 300 km is appropriate in general.

Positioning precision improvement is of great value. Thus, the analyses of the experimental results focused positioning precision with different ionospheric solutions in both static and dynamic scenarios. With the Australian ionospheric corrections generated on 1 January 2014, the evaluation was performed with both SPP and SF-PPP processing modes, based on modifications to the RTKLIB. The SPP solutions from 25 selected reference receivers have shown the decimetre RMS accuracy to be better than 19 cm for the East/North directions and 55 cm for the Up-component. With the same data sets and receivers, the SF-PPP mode yields RMS accuracy of better than 10 cm and 25 cm for the horizontal and vertical components

respectively. The dynamic experiment on the road scenario was conducted to evaluate the functionality of SIM on low-cost GNSS devices. This experiment demonstrates that SIM corrections works properly for low-cost receivers to do lane-level positioning.

5.2.3 Proposed CSR Method

A coordinate space representation is proposed in this thesis. That the coordinate bias at one station can improve the coordinates for nearby users was proved mathematically. This method has the potential to improve the positioning capability for SPP users, without investing too much about equipment and network construction. CSR differs from other differencing techniques, in that the raw measurements are not required either from server end or at user end. This means a lot to mobile phone users. The overall pattern of daily coordinate biases derived from the seven stations show great consistency. It demonstrated the value of this method.

Overall, this work demonstrates the promising potential for the Australia GNSS network to offer decimetre positioning services with SF GNSS receivers. This potential may support many new emerging applications over Australia, like ITS road safety control, electric tolling, UAV delivery, GIS data collection and even entertainment applications.

Bibliography

Ansari, K., Wang, C., Wang, L., & Feng, Y. (2013). Vehicle-to-vehicle real-time relative positioning using 5.9 GHz DSRC media. Paper presented at the Vehicular Technology Conference (VTC Fall), 2013 IEEE 78th.

Banville, S., Collins, P., Zhang, W., & Langley, R. B. (2014). Global and Regional Ionospheric Corrections for Faster PPP Convergence. Navigation, 61(2), 115-124.

Barr, A. (2013). Amazon testing delivery by drone, CEO Bezos says. Retrieved April, 22, 2014.

Black, H., & Eisner, A. (1984). Correcting satellite Doppler data for tropospheric effects. Journal of Geophysical Research: Atmospheres, 89(D2), 2616-2626.

Blanch, J. (2003). Using Kriging to bound satellite ranging errors due to the ionosphere. Stanford University.

Böhm, J., Niell, A., Tregoning, P., & Schuh, H. (2006). Global Mapping Function (GMF): A new empirical mapping function based on numerical weather model data. Geophysical Research Letters, 33(7)

Braasch, M. S., & Van Dierendonck, A. (1999). GPS receiver architectures and measurements. Proceedings of the IEEE, 87(1), 48-64.

Chen, X., Allison, T., Cao, W., Ferguson, K., Grünig, S., Gomez, V., Leandro, R. (2011). Trimble RTX, an innovative new approach for network RTK. Paper presented at the ION GNSS.

Collins, P. (2008, January). Isolating and estimating undifferenced GPS integer ambiguities. In Proc. ION NTM (pp. 720-732).

Conte, J. F., Azpilicueta, F., & Brunini, C. (2011). Accuracy assessment of the GPS-TEC calibration constants by means of a simulation technique. Journal of Geodesy, 85(10), 707-714.

Crespi, M., Mazzoni, A., & Brunini, C. (2012). Assisted Code Point Positioning at Sub-meter Accuracy Level with Ionospheric Corrections Estimated in a Local GNSS Permanent Network Geodesy for Planet Earth (pp. 761-768): Springer.

EL‐ARINI, M. B., Conker, R. S., Albertson, T. W., Reagan, J. K., Klobuchar, J. A., & Doherty, P. H. (1994). Comparison of Real‐Time Ionospheric Algorithms for a GPS Wide‐Area Augmentation System (WAAS). Navigation, 41(4), 393-414.

Feltens, J., Dow, J., Martín-Mur, T., Martínez, C. G., & Bernedo, P. (1998). ROUTINE PRODUCTION OF IONOSPHERE TEC MAPS AT ESOC-FIRST RESULTS.

Feng, Y., Gu, S., Shi, C., & Rizos, C. (2013). A reference station-based GNSS computing mode to support unified precise point positioning and real-time kinematic services. Journal of Geodesy, 87(10-12), 945-960.

Green, D., Gaffney, J., Bennett, P., Feng, Y., Higgins, M., & Millner, J. (2013). Vehicle positioning for C-ITS in Australia (background document).

GSA. (2015). 2015 GNSS Market Report. (4).

Gu, S. (2013). Research on the Zero-difference Un-combined Data Processing Models for Multi-frequency GNSS and Its Applications. Wuhan University.

Hernández-Pajares, M., Juan, J., Sanz, J., Orus, R., Garcia-Rigo, A., Feltens, J., . . . Krankowski, A. (2009). The IGS VTEC maps: a reliable source of ionospheric information since 1998. Journal of Geodesy, 83(3-4), 263-275.

Heo, Y., Yan, T., Lim, S., & Rizos, C. (2009). International standard GNSS real-time data formats and protocols. Paper presented at the IGNSS Symp.

Huo Guang, W. Z., Wang Siqi, Li Na. (2016, 10 January 2016). CES curtain fell: which products can really change lives? , from http://www.yicai.com/news/2016/01/4736896.html

IGS Data and Products. (2016). from http://igsws.unavco.org/components/prods.html

Kaplan, E. D., & Hegarty, C. J. (2005). Understanding GPS: principles and applications: Artech house.

Kee, C., Parkinson, B. W., & Axelrad, P. (1991). Wide area differential GPS. Navigation, 38(2), 123-145.

Klobuchar, J. A. (1987). Ionospheric time-delay algorithm for single-frequency GPS users. Aerospace and Electronic Systems, IEEE Transactions on(3), 325-331.

Komjathy, A., Sparks, L., Mannucci, A. J., & Coster, A. (2005). The ionospheric impact of the October 2003 storm event on Wide Area Augmentation System. GPS Solutions, 9(1), 41-50.

Kouba, J., & Héroux, P. (2001). Precise point positioning using IGS orbit and clock products. GPS Solutions, 5(2), 12-28.

Lanyi, G. E., & Roth, T. (1988). A comparison of mapped and measured total ionospheric electron content using global positioning system and beacon satellite observations. Radio science, 23(4), 483-492.

Li, Z., Fan, L., Yuan, Y., Verhagen, S., de Bakker, P., Yuan, H., & Zhong, S. (2014b). Mitigation of Ionospheric Delay in GPS/BDS Single Frequency PPP: Assessment and Application. 304, 477-499. doi: 10.1007/978-3-642-54743-0_39

Li, Z., Yuan, Y., Li, H., Ou, J., & Huo, X. (2012). Two-step method for the determination of the differential code biases of COMPASS satellites. Journal of Geodesy, 86(11), 1059-1076.

Mannucci, A., Wilson, B., Yuan, D., Ho, C., Lindqwister, U., & Runge, T. (1998). A global mapping technique for GPS ‐ derived ionospheric total electron content measurements. Radio science, 33(3), 565-582.

McCarthy, Dennis, D., & Petit, G. (2004). IERS conventions (2003): DTIC Document.

Minkwitz, D., Gerzen, T., Wilken, V., & Jakowski, N. (2014). Application of SWACI products as ionospheric correction for single-point positioning: a comparative study. Journal of Geodesy, 88(5), 463-478.

Misra, P., & Enge, P. (2006). Global Positioning System: Signals, Measurements and Performance Second Edition: Lincoln, MA: Ganga-Jamuna Press.

Øvstedal, O. (2002). Absolute positioning with single-frequency GPS receivers. GPS Solutions, 5(4), 33-44.

Parkinson, B. W., & Enge, P. K. (1996). Differential gps. Global Positioning System: Theory and applications., 2, 3-50.

Proakis, J. G. (2001). digital communication, 5th ed.: Wiley Online Library.

Rango, A., Laliberte, A., Herrick, J. E., Winters, C., Havstad, K., Steele, C., & Browning, D. (2009). Unmanned aerial vehicle-based remote sensing for rangeland assessment, monitoring, and management. Journal of Applied Remote Sensing, 3(1), 033542-033542-033515.

Rho, H., & Langley, R. B. (2007). Dual-frequency GPS precise point positioning with WADGPS corrections. NAVIGATION-LOS ANGELES AND WASHINGTON-, 54(2), 139.

Rizos, C. (1997). Principles and practice of GPS surveying: University of New South Wales.

Rizos, C. (2009). Network RTK Research and Implementation-A Geodetic Perspective. Positioning, 1(02).

RTCM. (2006). Standard 10403.1 for Differential GNSS (Global Navigation Satellite Systems) Services-Version 3. Radio Technical Commission for Maritime Services.

Saastamoinen, J. (1972). Atmospheric correction for the troposphere and stratosphere in radio ranging satellites. The use of artificial satellites for geodesy, 247-251.

Sardon, E., Rius, A., & Zarraoa, N. (1994). Estimation of the transmitter and receiver differential biases and the ionospheric total electron content from Global Positioning System observations. Radio science, 29(3), 577-586.

Satirapod, C., Rizos, C., & Wang, J. (2001). GPS single point positioning with SA off: how accurate can we get? Survey Review, 36(282), 255-262.

Schaer, S., Beutler, G., & Rothacher, M. (1998). Mapping and predicting the ionosphere. Paper presented at the Proceedings of the 1998 IGS Analysis Center Workshop, Darmstadt, Germany.

Schaer, S., Gurtner, W., & Feltens, J. (1998). IONEX: The ionosphere map exchange format version 1. Paper presented at the Proceedings of the IGS AC workshop, Darmstadt, Germany.

Shi, C., Gu, S., Lou, Y., & Ge, M. (2012). An improved approach to model ionospheric delays for single-frequency precise point positioning. Advances in Space Research, 49(12), 1698-1708.

Van Diggelen, F. S. T. (2009). A-GPS: Assisted GPS, GNSS, and SBAS. Artech House.

Wahr, J. M. (1981). The forced nutations of an elliptical, rotating, elastic and oceanless Earth. Geophysical Journal International, 64(3), 705-727.

Wanninger, L. (1993). Effects of the Equatorial Ionosphere on GPS. GPS World.

Wu, J. T., Wu, S. C., Hajj, G., Bertiger, W. I., & Lichten, S. M. (1993). Effects of antenna orientation on GPS carrier phase. Manuscripta geodaetica, 18, 91-91.

Wu, X., Hu, X., Wang, G., Zhong, H., & Tang, C. (2013). Evaluation of COMPASS ionospheric model in GNSS positioning. Advances in Space Research, 51(6), 959-968.

Wübbena, G., Bagge, A., & Schmitz, M. (2001). Network-based techniques for RTK applications. Paper presented at the GPS Symposium, GPS JIN.

Wübbena, G. (2012). RTCM State Space Representation (SSR) Overall Concepts Towards PPP-RTK. Paper presented at the PPP-RTK & Open Standards Symposium, Frankfurt, Germany.

Xin, Y. (2016). DJI agricultural layout:plant protection UAV being relieased at a price of RMB 52999. from http://tech.huanqiu.com/original/2016-03/8745412.html

Yuan, Y., Huo, X., Ou, J., Zhang, K., Chai, Y., Wen, D., & Grenfell, R. (2008). Refining the Klobuchar ionospheric coefficients based on GPS observations. Aerospace and Electronic Systems, IEEE Transactions on, 44(4), 1498-1510.

Zandbergen, P. A. (2009). Accuracy of iPhone locations: A comparison of assisted GPS, WiFi and cellular positioning. Transactions in GIS, 13(s1), 5-25.

Zhang, H., Gao, Z., Ge, M., Niu, X., Huang, L., Tu, R., & Li, X. (2013). On the convergence of ionospheric constrained precise point positioning (IC-PPP) based on undifferential uncombined raw GNSS observations. Sensors (Basel), 13(11), 15708-15725. doi: 10.3390/s131115708

Zumberge, J., Heflin, M., Jefferson, D., Watkins, M., & Webb, F. (1997). Precise point positioning for the efficient and robust analysis of GPS data from large networks. Journal of Geophysical Research: Solid Earth (1978–2012), 102(B3), 5005-5017.